Designing angle-independent colored materials using light scattering by aggregate particles

Yui Naoi

Department of Molecular and Macromolecular Chemistry
Nagoya University

2020

Contents

Chapter III
Characterization of Colloidal Amorphous Arrays Prepared by Uniaxial Pressure Application

Chapter IV
Angle-Independent Colored Materials with Mie Scattering and Rayleigh Scattering in Response to Pressure

Chapter I

General Introduction

1-1. Introduction

Our lives involve various colors. The colored materials in our lives can be divided into two types. The common colored materials in our lives are colored materials that absorb light. Representative materials include organic dyes and pigments. Organic dyes and pigments show various brilliant colors. However, they are disadvantageous as colored materials because they decompose and decolorize under the influence of sunlight and chemical substances. The occurrence of health hazards due to harmful organic materials has been reported. Thus, the regulations on organic colored materials have become strict: the ETAD (Ecological and Toxicological Association of Dyes and Organic Pigments Manufacturers) was established as an international organization in Europe, and severe restrictions have been imposed on the use of organic colored materials.

Organic dyes and pigments are not perfectly safe, which is why their use raises concerns.

The second type of representative colored material includes inorganic pigments. Although inorganic pigments are excellent in terms of durability and chromogenic properties, many of them contain highly toxic heavy metals[1]. Therefore, obtaining licenses for their use is difficult. As a matter of course, colored materials that absorb light have been studied to overcome the extinction of color and toxicity. However, their use is strictly limited by law.

The preparation of safer colored materials is needed because colored materials that absorb

light may not be permanently usable[2,3].

Recently, colored materials involving physical phenomena such as scattering, interference and resonance have been attracting attention instead of materials that absorb light.

If safe materials are selected for scatterers, then colored materials based on these physical phenomena could be used as human-friendly and environmentally friendly colored materials. Typical materials include structural color materials[3-11]. Structural colors are caused by scattering, interference and resonance arising from the microstructure with a size comparable to the wavelength of light on the surface of the material. Structural color can be observed in nature, for example, in feathers, beetles and animals' bodies.

Some colors are caused by physical phenomena different from that of structural color in nature. In contrast to the structural color generated from an aggregate of substances with different refractive indices, color can be generated by the scattering of light from a single particle. The scattering phenomena include Rayleigh scattering[12], showing a sky-blue color, and Mie scattering[13], showing a white cloud color . Although application research for colored materials has not progressed compared with that for structural colors, the phenomenon could lead to human-friendly and environmentally friendly colored materials.

This thesis suggests guiding the design of angle-independent colored materials by using scattering, interference and resonance of light involving aggregates composed of safe materials.

1-2. Light scattering from particles

1-2-1. Rayleigh scattering

Rayleigh scattering is light scattering that occurs when the particle size is smaller than the light wavelength[12,14]. Lord Rayleigh obtained an approximate solution in the case of a wavelength far smaller than the radius of a sphere to demonstrate the blue of the sky in 1881[12]. Therefore, this scattering is called “Rayleigh scattering”. Rayleigh scattering is caused by particles of any shape if the particle size is smaller than the light wavelength. In other words, scattering occurs regardless of whether the particles are spherical or nonspherical. As shown in Figure 1-1(a), the light is scattered not only in the anterior direction but also backward with respect to the irradiation direction. The reflectance of scattered light is inversely proportional to the fourth power of the light wavelength. Thus, shorter wavelength light is reflected. Therefore, blue and purple colors are visualized by Rayleigh scattering. As previously mentioned, the representative color caused by Rayleigh scattering is sky blue (Figure 1-1(b)). The blue color of the sky is caused by blue wavelength light being scattered by air molecules smaller than the light wavelength. Hence, what is the cause of the red color of the sunset?

Although the red color is a visualization of long wavelength light, the color occurs from Rayleigh scattering (Figure 1-1(c)). When the sun sets over the horizon, the distance between the sun and the ground is the longest.

At this time, the blue light is scattered by molecules in the air, and the scattered light

(a)

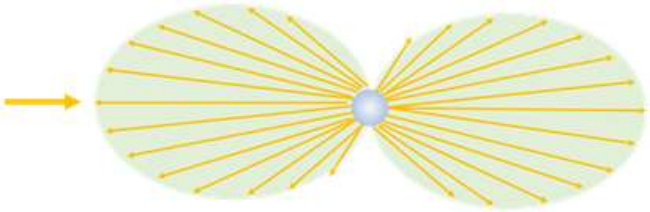

(b)

(c)

Figure. 1-1 (a) A figure of Rayleigh scattering from a particle. (b) A photograph of blue sky. (reproduced with permission from https://www.beiz.jp) (c) A photograph of sunset. (reproduced with permission from https://www.beiz.jp)

does not reach the surface of the earth. Thus, red light reaches the surface of the earth, so the sunset is seen as red.

1-2-2. Mie scattering

Mie scattering occurs for spherical particles. Gustav Mie obtained an exact solution of the scattering of light by a sphere in 1908[13]. Therefore, this scattering phenomenon is called “Mie scattering”.

Mie scattering occurs when the particle size of the scatterer is comparable to the wavelength of light. The behavior of light scattered by Mie scattering is shown in Figure 1-2(a). Forward scattering is enhanced compared with backward scattering. The larger the particle size is, the more the forward scattering is enhanced. A familiar example caused by Mie scattering is cloud whiteness (Figure 1-2 (b)). Light with a wavelength comparable to the particle size is scattered by Mie scattering. Therefore, Mie scattering can be used for colored materials such as pigments and biomarkers because changing the hue is easy[15-19]. Furthermore, light scattered by this phenomenon exhibits various interesting behaviors depending on the particle size and refractive index, as shown in the following sections.

(a)

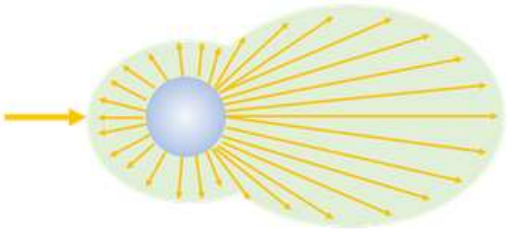

(b)

Figure. 1-2 (a) A figure of Mie scattering from a particle. (b) A photograph of blue sky and white clouds. (reproduced with permission from https://www.beiz.jp)

1-2-3. Single particle scattering

In the case of a low refractive index particle causing Mie scattering, the explanation is that light irradiating the particle reaches the inner wall of the particle, and the reflected light interferes in the optical path.

Manoharan et al. argued that such scattering causes submicron-sized particles to have a low refractive index (n = 1.4). They called this phenomenon "single particle scattering"[20]. They argued that reflected light beams interfere similar to thin film interference, and the interfered light beams are scattered backward unlike in Mie scattering, as shown in Figure 1-3(a). In addition, they calculated the angle dependence of this scattering from an independent particle. As a result, they reported that the light scattering shows angle dependence.

1-2-4. Mie resonances (whispering gallery mode)

In the case of high refractive index particles and micrometer-size particles, light with a wavelength comparable to the particle size circumnavigates near the surface of the particle similar to total internal reflection. This phenomenon is called Mie resonances (other name: whispering gallery mode)[21-23]. Mie resonances have been studied for application to displays, lasers and resonators due to the ability to enhance the light confinement effect and light emission[24-32].

1-2-5. Relationship between Mie scattering and aggregates

The phenomenon of Mie scattering from aggregates of particles has been discussed by

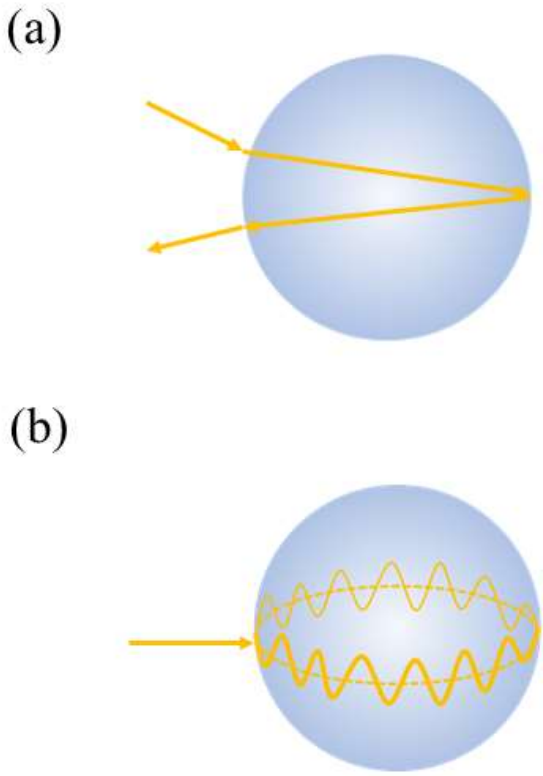

Figure 1-3. (a) A photograph of Single particle scattering. (b) A photograph of Mie resonances (Whispering gallery mode).

many researchers. Lopez and colleagues argued that when particles causing Mie resonance form aggregates, the light is confined, which produces enhanced light similar to a random laser[33, 34]. As the name random laser implies, the aggregates exhibit laser emission in a random direction.

On the other hand, Manoharan and Kim thought that Mie scattering occurs from an independent single particle and that the aggregate form has no effect.

The phenomena occurring upon the formation of an aggregate composed of particles causing Mie scattering remain a mystery[19.20].

1-3. Structural color

When the order of the size of a microstructure composed of two different refractive index materials is comparable to that of visible light wavelengths, the light undergoes reflection, resonance and scattering.

The color caused by this phenomenon is called "structural color"[3-11]. Structural color is ordinarily observed in nature. The color of morpho butterflies[35, 36], opals[37,38], known as jewels, and feathers[39] are caused by structural color. Structural color does not fade as long as the structure and contrast of the refractive indices do not change. Materials displaying structural color could become low-cost, human-friendly and environmentally friendly colored materials.

Attempts to produce structural color using artificial materials has been made since olden days. A well-known method for producing structural color materials is gravitational sedimentation of particle suspensions[40].

In addition, the production of characteristic structural color materials by various methods, such as spin coating[36-38], centrifugation[39], and those using microfluidic devices[40], has been reported.

1-3-1. Colloidal crystals

An aggregate formed by monodisperse colloidal particles with long-range order is called a "colloidal crystal"[46-50](Figure 1-4(a)). When the order of the size is comparable to that of visible light wavelengths, the light is selectively reflected. The wavelength of light scattered from colloidal crystals is determined by combining Snell's formula and Bragg's formula considering the average refractive index of the colloidal crystal.

$$\lambda_{max}=2(a/m)(n_{ave2}-\sin\theta^{2})^{1/2}$$

where a denotes the lattice spacing, m denotes the order of the Bragg reflection, n denotes average the refractive index of the colloidal crystal and θ denotes the incident angle. When m = 1, the reflection intensity is the highest.

The average refractive index n_{ave} of a colloidal crystal is the sum of the refractive indices of the colloidal particles composing the crystal and the medium. The value can be calculated as follows:

$$n_{ave} = \Sigma n_i^2 \phi_i$$

where n_i and ϕ_i denote the refractive index and volume fraction of each portion i. Colloidal crystals show brilliant colors, similar to morpho butterflies and opals.

Moreover, the reflected light wavelength can be tuned by changing the refractive index of the particles, particle size and interparticle distance. Therefore, these crystals are

(a)

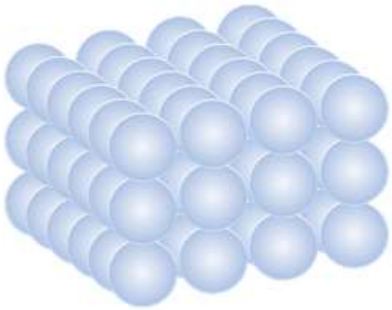

(b)

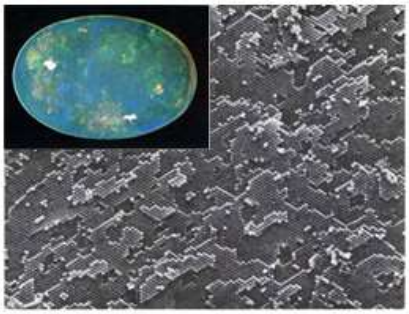

Figure 1-4. (a) Colloidal Crystal. (b) A photograph and electron micrograph of Opal (reproduced with a permission from [38] @ 1976 Scientific American) .

expected to apply to not only pigments but also sensors.

However, the color shows angle dependence when changing the viewing angle and incident angle, so the structure has anisotropy.

In the case of sensors, the use of colloidal crystals is difficult if the color derived from them shows angle dependence. The angle dependence of the color arising from colloidal crystals is a defect when used as colored materials.

1-3-2. Colloidal amorphous arrays

An aggregate formed by colloidal particles with short-range order is called a "colloidal amorphous array"[51-70] (Figure 1-5(a)). These arrays have an isotropic structure and scatter specific light with a wavelength comparable to the size order in all directions, called "coherent light scattering". When particles form aggregates, multiple scattering occurs because light in the entire visible light range is scattered many times between the particles. The research on the application of colloidal amorphous arrays as colored materials has been delayed because researchers have not paid attention to arrays composed of silica and polystyrene particles showing a whitish color.

However, colloidal amorphous arrays are commonly found in nature, and the structural color resulting from colloidal amorphous aggregates is seen in bird wings and dragonfly bodies, as shown in Figure 1-5 (b). Recently, the structural color caused by colloidal amorphous arrays was found to show vivid colors in a black background, which reduces multiple scattering.

Colloidal amorphous arrays have been reported to show angle-independent color under

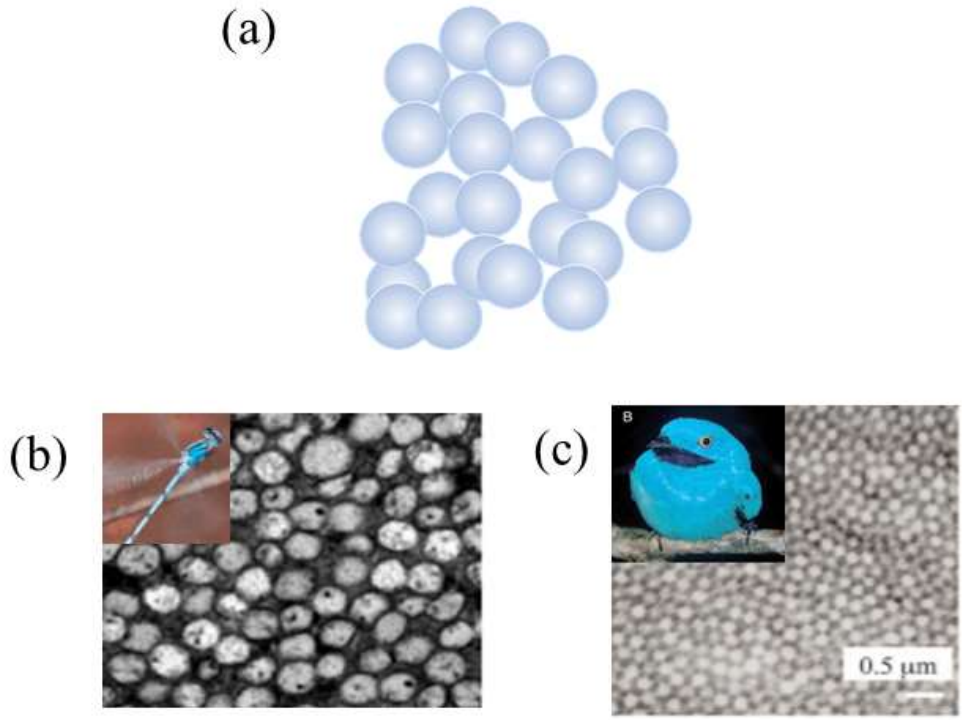

Figure 1-5. (a) Colloidal amorphous array. (b) A photograph and electron micrograph of dragon fly (reproduced with a permission from [35] @ 2006 The Journal of Experimental Biology). (c) A photograph and electron micrograph of feather of a bird (reproduced with a permission from [39] @ 2014 Japanese Journal of Optics).

natural light. The term “natural light” means the conditions in which a sample is illuminated from all directions, such as by sunlight or fluorescent light. Colloidal amorphous arrays show angle-independent color under natural light because incident light from all directions cumulatively contributes to coherent light scattering. As a result, the scattering peak from the colloidal amorphous array becomes broad, and the arrays display pale colors and the same hue regardless of from which angle they are viewed.

However, when light is irradiated only from a specific direction onto the colloidal amorphous arrays, their hues exhibit angle dependence.

1-4. Scope of this thesis

1-4-1. Objectives

Colored materials, involving scattering, reflection and resonance of light, could become low-cost, human-friendly and environmentally friendly colored materials. Colored materials based on these phenomena have many advantages; however, there are some disadvantages and unclear points.

Rayleigh scattering strongly scatters shorter wavelength light, but the reflectance of longer wavelength light is low. Therefore, changing the hue of colored materials by using Rayleigh scattering is difficult. For Mie scattering, the studies have progressed. Many examples of the preparation of pigments using this scattering have been reported. However, the effect that occurs when particles causing Mie scattering form aggregates is not understood. Researchers have a difference in opinion as to this unclear point.

Colloidal crystals, which have been studied for use as colored materials and optical

materials for a long time, display vivid colors. However, their disadvantage is that they show angle-dependent colors.

In contrast, colloidal amorphous arrays show angle-independent color under natural light. However, the arrays show angle dependence under specific conditions. Moreover, the history of their study is short.

This thesis proposes new guidelines for the material design of colored materials showing angle independence using light scattering.

1-4-2. Outline of this thesis

This thesis consists of six chapters, Chapters I to VI.

In chapter II, guidelines for the preparation of perfectly angle-independent colored materials are suggested by forming a colloidal amorphous array composed of particles causing Mie scattering. The angle dependence of the color of fine particles is reported to disappear when the fine particles causing Mie scattering aggregate. After that, angle-independent colored materials are successfully prepared by positioning the Mie scattering peak caused by colloidal aggregates in the visible light range based on the Mie scattering property.

In chapter III, an association between Mie scattering and colloidal aggregates is revealed because the intensity and position of the Mie scattering peak caused by colloidal aggregates differ from those in the Mie scattering spectra caused by an independent single particle. The Mie scattering spectra caused by an independent single particle are compared with the Mie scattering spectra caused by pellet-like colloidal amorphous

arrays.

Furthermore, in chapter III, anisotropy is induced in the structure by applying a uniaxial force to produce a colloidal amorphous aggregate. A new route for producing a structural color material with less angle dependence than previously achieved is established.

In chapter IV, a colored material with changing hue in response to pressure is prepared by causing a phenomenon change from Mie scattering to Rayleigh scattering. Aggregates are prepared by uniaxially pressing soft particles covered with titanium oxide. Brilliant colored materials exhibiting Rayleigh scattering are successfully prepared by dispersing titanium, causing uniform Rayleigh scattering.

In chapter V, a colloidal crystal showing an angle-independent color is prepared by using high refractive index CeO_2/polyvinylpyrrolidone (PVP) particles based on the Bragg-Snell law.

Finally, this thesis is summarized and a future outlook is provided in chapter VI.

References

[1] T. Masui, S. Fukukawa, N. Imanaka, *Chem. Lett.*, **35**, 1032-1033 (2006).

[2] Sustainable Development Goals of United Nations Development Programe.(https://www.undp.org/content/undp/en/home/sustainable-development-goals.html).

[3] Y. Takeoka, *Chem. Commun*., **54** (39), 4905-4914(2018).

[4] M. Srinivasarao, *Chem. Rev.*, **99**, 1935-1961(1999).

[5] A. R. Parker, *J. Opt. A : Pure Appl. Opt.*, **2**, R15-R28)(2002).

[6] S. Kinoshita, S. Yoshioka, Y. Fujii, N. Okamoto, *Forma*, **17**, 103-121(2002).

[7] P. Vukusic, J. R. Sambles, *Nature* , **424,** 852-855 (2003).

[8] S. Kinoshita, S. Yoshioka, *ChemPhysChem*, 6, 1442-1459(2005).

[9] A. R. Parker, N. Martini, *Opt. Laser Technol*., **38**, 315-322(2006).

[10] J. T. Bagnara, P. J. Fernandez, R. Fujii, *Pigment Cell Res.*, **20**, 14-26(2007).

[9] S. Kinoshita, S. Yoshioka, J. Miyazaki, *Rep. Prog. Phys.* , **71**, 076401 (2008).

[10] A. Seeboth, D. Lotzsch, R. Ruhmann, O. Muehling, *Chem. Rev.*, **114** (5), 3037-30682014.

[11] Y. Takeoka, *J. Mater. Chem. C*, **1** (38), 6059-6074(2013).

[12] L. Rayleigh, *Scientific Papers*, **5** : 617(1912).

[13] G. Mie, Ann. Phys., **25**, 377-455(1908).

[14] D. Ge, L. Yang, G. Wua and S. Yang, *J. Mater. Chem. C*, 2014,**2**, 4395-4400.

[15] M. Retsch, M. Schmelzeisen, H-J. Butt, and E. L. Thomas, *Nano Lett.*, **11**, 1389–1394 (2011).

[16] L. A. Fielding, O. O. Mykhaylyk, A. Schmid, D. Pontoni, S. P. Armes, and P. W. Fowler, *Chem. Mater.*, **26**, 1270−1277 (2014).

[17] W. Yuan, N. Zhou, L. Shi, and K-Q. Zhang, *ACS Appl. Mater. Interfaces*, **7**, 14064−14071 (2015).

[18] S. Cho, T. S. Shim, J. H. Kim, D-H. Kim, and S-H. Kim, *Adv. Mater.*, **29**, 1700256 (2017).

[19] S-H. Kim, V. Hwang, S. G. Lee, J-W. Ha, V. N. Manoharan, and G-R. Yi, *Small*, **15**, 1900931 (2019).

[20] S. Magkiriadou, J-G. Park, Y-S. Kim, and V. N. Manoharan, *Phys. Rev. E.*, 2014, 90 (6).

[21] Y. Yamamoto and R. E. Slusher: Phys. Today Junuary, 66 (1993).

[22] R. K. Chang and A. J. Campillo. ed.: Optical processes in microcavitites (World Scientific Publishing, Singapore, New Jersey, London, Hong Kong, 1996).

[23] F. Vollmer and S. Arnold, *Nat.method*, **5**, 591-596 (2008).

[24] D.S. Weiss, V. Sandoghdar, J. Hare, V. Lefevre-Seguin, J.-M. Raimond, and Haroche, Optics Letter, 20, 1835-1837 (1995).

[25] L. Shi, J. T. Harris, R. Fenollosa, I. Rodriguez, X. Lu, B. A. Korgel and F. Meseguer, *Nat.Commun*., **4**, 1-7 (2013).

[26] T. A. Kumara, M. A. Mohiddon, N. Dutta, Nirmal K. Viswanathan, and S. Dhara, *Appl. Phys. Lett.*, **106**, 0511101 (2015).

[27] Montesdeoca, D.; Bayat, F.; Espinha, A.; Blanco, A.; Pecharroman, C.; Lopez, C., Monodisperse Silica Spheres Ensembles with Tailored Optical Resonances in the Visible. *Part. Part. Syst. Char.*, **33** (12), 871-877(2016).

[28] M. Naffouti, T. David, A. Benkouider, L Favre, A. Ronda, I. Berbezier, S. Bidault, N. Bonodd and M. Abbarchi, *Nanoscale*, **8**, 2844-2849 (2016).

[29] S. Kushida, D. Okada, F. Sasaki, Z-H. Lin, J-S. Huang, Y. Yamamoto, *Adv. Opt. Mater.*, **5**, 1700123 (2017).

[30] J. Zhou, A. Panday, Y. Xu, X. Chen, L. Chen, C. Ji, L. J. Guo, *Phys. Rev. Lett.*, **120**, 253902 (2018).

[31] K. Yoshihara, M. Sakamoto, H. Tamamitsu, M. Arakawa, K. Saitow, *Adv. Opt. Mater.*, **6**, 1800462 (2018).

[32] M. L. D. Marco, S. Semlali, B. A. Korgel, P. Barois, G. L. Drisko, C. Aymonier, *Angew. Chem., Int. Ed.*, 2018, **57**, 2-23.

[33] S. Gottardo, R. Sapienza, P. D. García, A. Blanco, D. S. Wiersma and Cefe López, *Nature Photonics*, **2**, 429–432(2008).

[34] R. Sapienza, P. D. Garcia, J. Bertolotti, M.D. Martin, Á. Blanco, l. Vina, C. Lopez and D, Wiersma, *Phys.Rev.Lett.* **99**. 233902 (2007).

[35] R.O. Prum, T. Ouinn and R. Torres, *J. Exp. Biol.*, **209**, 748-765 (2006).

[36] A. Saito, Sci. Tecnol. *Adv. Mater.*, **12**, 064709 (13pp) (2011).

[37] J. V. Sanders, *Nature*, **204**, 1151-1153 (1964).

[38] P. J. Darragh, A. J. Gaskin and J. V. Sanders, *Scientific American*, **234**, 84-95 (1976).

[39] Y.Takeoka , *Japanese journal of optics*, **43**, 516-523 (2014).

[40] S. Furumi, H. Fudouzi, and T. Sawada, Laser & Photon. Rev.4, No.2, 205–220 (2010).

[41] A. Mihi M. Ocaña H. Míguez, *Adv. Mater.*, **18**, 2244-2249 (2006).

[42] M. Giuliani, W. Gonzalez-Vinas, K. M. Poduska, and A. Yethiraj, *A. Phys. Chem. Lett.*, **1**, 1481-1486 (2010).

[43] P. Colson, R. Cloots, C. Henrist, *Langmuir*, **27**, 12800-12806 (2011).

[44] Katagiri, K.; Tanaka, Y.; Uemura, K.; Inumaru, K.; Seki, T.; Takeoka, Y., Structural color coating films composed of an amorphous array of colloidal particles via electrophoretic deposition. *Npg Asia Mater*, **9**. 28, (2017).

[45] Jin-Gyu Park, Shin-Hyun Kim, Sofia Magkiriadou, Tae Min Choi, Young-Seok Kim, and Vinothan N. Manoharan*

[46] Kohri, M., Artificial melanin particles: new building blocks for biomimetic structural coloration *Polym J.,* 2019.

[47] Y. N. Xia , B. Gates , Y. D. Yin and Y. Lu , *Adv. Mater*., **12** , 693 -713(2000).

[48] Y. N. Xia , B. Gates and Z. Y. Li , *Adv. Mater*., **13** , 409 -413 (2001).

[49]F. Li , D. P. Josephson and A. Stein , *Angew. Chem., Int. Ed*., **50** , 360 -388(2011).

[50] Y. Z. A. Zhang , J. X. Wang , Y. Huang , Y. L. Song and L. Jiang , *J. Mater. Chem.*, 2011, **21** , 14113 -14126.

[51] S. H. Kim , S. Y. Lee , S. M. Yang and G. R. Yi , *NPG Asia Mater.*, 2011, **3** , 25 -33.

[52] Y. Takeoka, M. Honda, T. Seki, M. Ishii, H. Nakamura, *ACS Appl. Mater. Interfaces*, 2009, **1**, 982-986.

[53] M. Harun-Ur-Rashid, A. Bin. Imran, T. Seki, M. Ishi, H. Nakamura, Y. Takeoka, *ChemPhysChem*, 2010, **11**, 579-583.

[54] J. D. Forster, H. Noh, S. F. Liew, V. Saranathan, C. F. Schreck, L. Yang, J. G. Park, R. O. Prum, S. G. J. Mochrie, C. S. O'Hern, H. Cao, E. R. Dufresne, *Adv. Mater.*, 2010, **22**, 2939-2944.

[55] P. D. Garcia, R. Sapienza, C. Lopez, *Adv Mater.*, 2010, **22** (1), 12-19.

[56] I. Lee, D. Kim, J. Kal, H. Baek, D. Kwak, D. Go, E. Kim, C. Kang, J. Chung, Y. Jang, S. Ji, J. Joo, Y. Kang, *Adv. Mater.*, 2010, **22** (44), 4973-4977.

[57] S. F. Liew, J. Foster, H. Noh, C. F. Schreck, V. Saranathan, X. Lu, L. Yang, R. O. Prum, C. S. O'Hern, E. R. Dufresne, H Cao, *Opt. Express*, 2011, **19**, 8208-8217.

[58] Y. Takeoka, S. Yoshioka, A. Takano, S. Arai, N. Khamin, H. Nishihara, M. Teshima, Y. Ohtsuka, T. Seki, *Angew. Chem., Int. Ed.*, 2013, **52**, 7261-7265.

[59] L. Shi, Y. F. Zhang, B. Q. Dong, T. R. Zhan, X. H. Liu, J. Zi, *Adv. Mater.*, 2013, **25** (37), 5314-5320.

[60] S. Yoshioka and Y. Takeoka, *ChemPhysChem*, 2014, **15**, 2209-2215.

[61] D. T. Ge, L. L. Yang, G. X. Wu, S. Yang, *J. Mater. Chem. C*, 2014, **2** (22), 4395-4400.

[62] D. Montesdeoca, F. Bayat, A. Espinha, A. Blanco, C. Pecharroman, C. Lopez, *Part. Part. Syst. Char.*, 2016, **33** (12), 871-877.

[63] I. Yoo, J. Hyon, S. Song, Y. Kang, *Sci. Adv. Mater.*, 2017, **9** (2), 238-243.

[64] G. J. Aubry, L. Schertel, M. D. Chen, H. Weyer, C. M. Aegerter, S. Polarz, H. Colfen, G. Maret, *Phys. Rev. A,* 2017, **96** (4), 043871.

[65] M. Iwata, M. Teshima, T. Seki, S. Yoshioka, Y. Takeoka, *Adv. Mater.*, 2017, **29** (26), 1605050.

[66] P. Shi, F. Wang, J. F. Zhu, H. B. Yang, Y. Wang, Y. Fang, B. Zhang, J. H. Wang, *J. Eur. Ceram. Soc.*, 2018, **38** (4), 2228-2233.

[67] S. Y. Lee, H. Kim, S. H. Kim, H. A. Stone, *Phys. Rev. Appl*., 2018, **10** (5), 054003.

[68] G. L. Shang, L. Maiwald, H. Renner, D. Jalas, M. Dosta, S. Heinrich, A. Petrov, M. Eich, *Sci. Rep.*, 2018, **8**, 7804.

[69] L. Schertel, L.Siedentop, J. M. Meijer, P. Keim, C. M. Aegerter, G. J. Aubry, G. Maret, *Adv. Opt. Mater.*, 2019, **7** (15), 1900442.

[70] M. Kohri, Y. Tamai, A. Kawamura, K. Jido, M. Yamamoto, T. Taniguchi, K. Kishikawa, S. Fujii, N. Teramoto, H. Ishii, D. Nagao, *Langmuir*, 2019, **35** (16), 5574-5580.

Chapter II

Development of Angle-Independent Colored Material Using a Colloidal Amorphous Array

2-1. Introduction

In recent years, colloidal amorphous arrays, in which monodisperse colloidal particles form an aggregate with short-range order, were found to be colored materials with a low angle dependence under natural light[1-6]. The term "natural light" means the conditions in which a sample is illuminated from all directions, such as by sunlight or fluorescent light. Colloidal amorphous arrays show angle-independent color under natural light because incident light from all directions cumulatively contributes to coherent light scattering. As a result, the scattering peak from the colloidal amorphous array becomes broad, and the arrays display the same hue regardless of from which angle they are viewed[6]. However, when light is irradiated only from a specific direction onto the colloidal amorphous arrays, their hues exhibit angle dependence[3].

In this study, we found a light scattering peak in the scattering spectrum observed from colloidal amorphous arrays, showing no angle dependence, on the shorter wavelength side of the scattering peak caused by the existence of short-range order. These peaks are caused by "Mie scattering" because the peaks shift when changing the particle size[7].

By using this light scattering phenomenon, we introduce the possibility of developing a colored material displaying a hue with angle independence even under the condition of light irradiation from one direction.

2-2. Experimental section

2-2-1. Materials

Fine particles composed of silica purchased from Fuji Chemical Co., Ltd. as the main component with average particle sizes of 280 nm, 360 nm, and 650 nm were used as colloidal particles. The coefficient of variation for the size distribution of each colloidal particle was 4.6%, 3.9%, and 4.0%, respectively.

Carbon black (CB) particles (average diameter of primary particles: 28 nm) provided by Tokai Carbon Co., Ltd. were used in this study.

2-2-2. Preparation of colloidal amorphous arrays

In this study, a spray method was used to easily prepare colloidal amorphous arrays composed of monodisperse colloidal particles[16,17]. CB was also used to prevent multiple scattering of light from the obtained colloidal amorphous arrays.

The typical preparation method of colloidal amorphous arrays was as follows. Fine silica particles (6 g) and CB (0.01 g) were stirred to uniformly disperse them in methanol (9 g) to prepare a suspension. Using an air spray system, the obtained suspension was sprayed on a glass substrate approximately 30 cm away (Scheme 2-1). As the methanol evaporated during the spraying of the suspension, the fine silica particles and CB formed secondary particles. As a result, a deposited film comprising secondary particle aggregates of the fine silica particles with a small amount of CB was obtained on the glass substrate. The thickness of the resulting film was approximately 1 mm.

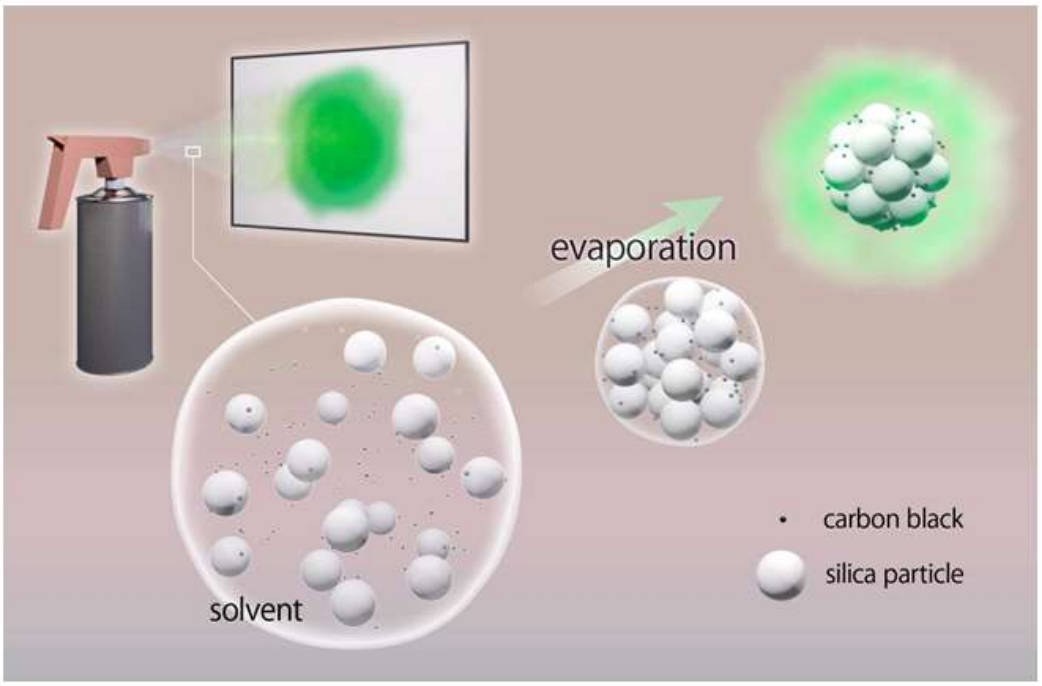

Scheme 2-1. Schematic diagram of the spray method to prepare colloidal amorphous arrays composed of the secondary particles.

2-2-3. Appearance observations of colloidal amorphous arrays

A photograph showing the appearance of the colloidal amorphous arrays was obtained using a digital camera. For observation of the arrangement of the fine silica particles in the colloidal amorphous arrays, a tabletop microscope (MiniScope TM3000) manufactured by Hitachi High Technology Co., Ltd. was used. The surfaces of the colloidal amorphous arrays were coated with a Au - Pd layer with a thickness of approximately 10 nm and were observed with an acceleration voltage of 15 kV.

2-2-4. Measurement of scattering spectra

For measurement of the scattering spectra of the colloidal amorphous arrays, a scattering spectrum measuring apparatus with a goniometer and a scattering spectrum measuring apparatus with an integrating sphere (JASCO Spectra Manager ™ for V600 series by JASCO Corporation) were used. The light-shielded state was used as the baseline, and the light from the light source was taken as 100%. The scattering spectra were measured with light incident from a direction perpendicular to the surface of the deposited films, and the position of the detector was changed from an angle of 0° to 90° with respect to the incident light direction.

2-3. Results and discussion

2-3-1. Scattering spectra of membranes composed of secondary particles

Secondary particles forming colloidal amorphous arrays on a glass substrate in the form of a film obtained by spraying a methanol suspension of submicron-size fine silica

particles and CB were already reported[16]. Figure 2-1 (a), Figure 2-1 (b), Figure 2-1 (c), and Figure 2-1 (d) show the angle dependence of the scattering spectra of the films composed of fine silica particles with an average size of 280 nm or 360 nm. The scattering peak observed at 510 nm (the first peak: coherent light scattering) in the scattering spectrum observed at a measurement angle of 0° for the film composed of 280 nm fine silica particles is caused by the coherent scattering of light due to the presence of the short-range order in the colloidal amorphous array. Since the coherent scattering peak is observed in the visible light region, this film exhibits a structural color. Generally, the wavelength range of visible light is from 380 nm to 780 nm. As the angle between the incident light direction and the observation direction increases, the position of the first peak caused by coherent scattering shifts to a shorter wavelength. That is, under the irradiation of directional light, which is a condition for general scattering spectrum measurement, an angle dependence occurs in the hue of the observed structural color. However, for this film, another scattering peak is also observed at 283 nm on the shorter wavelength side of the coherent scattering peak. Hereinafter, the peak due to coherent scattering is called the "first peak", and the peak observed on the shorter wavelength side is called the "second peak" due to Mie scattering. Figure 2-1 (b) shows a plot of the observation angle dependence of the positions of both peaks. Compared to the first peak, the position of the second peak shows no observation angle dependence.

In the case of the film comprising 360 nm fine silica particles, both peaks appear on the longer wavelength side of the peaks observed for the film composed of 280 nm fine particles. When the observation angle is 0°, these peaks are observed at 670 nm and 373

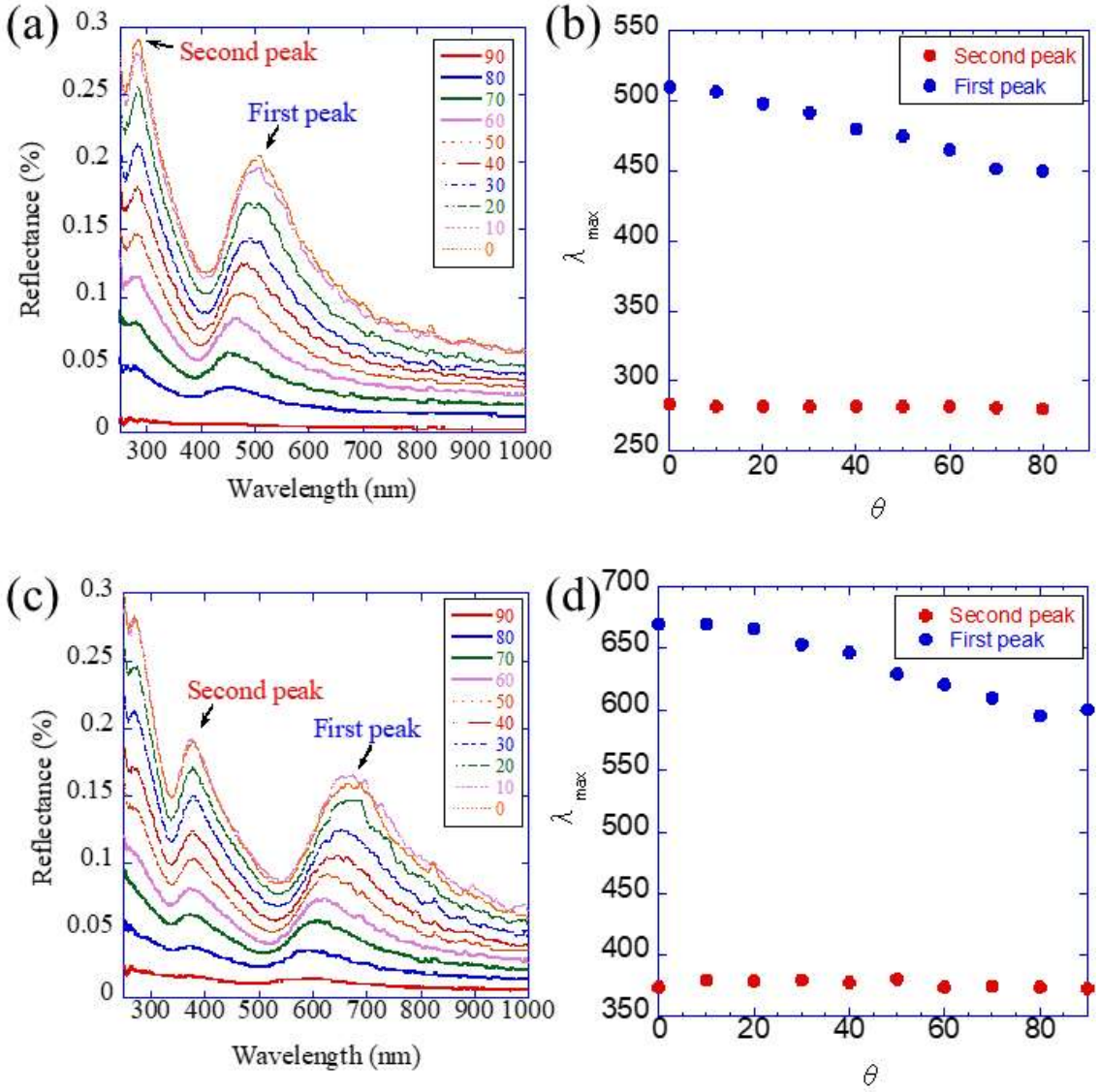

Figure 2-1. (a) Angle-dependent scattering spectra of membrane composed of silica particles with the average particle diameter (D_{ave}) = 280 nm and CB. (b) Plots of the positions of the first and the second peaks from (a) versus the detection angle. (c) Angle-dependent scattering spectra of membrane composed of silica particles with D_{ave} = 360 nm and CB. (d) Plots of the positions of the first and the second peaks from (c) versus the detection angle.

nm (Figure 2-1 (c)). When plotting the angle dependence of the positions of both peaks according to Figure 2-1 (b), the first peak shifts to a shorter wavelength with increasing observation angle, but the position of the second peak does not show any angle dependence (Figure 2-1 (d)). As described above, the second peak of the scattering spectra observed from the colloidal amorphous arrays shows that as the size of the fine silica particles increases, its position shifts to a longer wavelength, and the peak position does not show angle dependence even under observation with directional light irradiation. Therefore, a colloidal amorphous array using fine silica particles with a larger size was prepared for making a colored material in which the hue does not change even under directional light irradiation.

2-3-2. Preparation of membranes composed of large particles

Figure 2-2 shows a photograph of the film composed of the secondary particles formed from fine silica particles with an average size of 650 nm and CB. The resulting membrane is grayish-turquoise. Electron microscopic observation revealed that the fine silica particles formed secondary particles and accumulated (Figure 2-3). Fourier transformation of the surface image of the secondary particles resulted in a circular pattern, as shown in the inset of Figure 2-3. This result shows that the fine silica particles form secondary particles with short-range order.

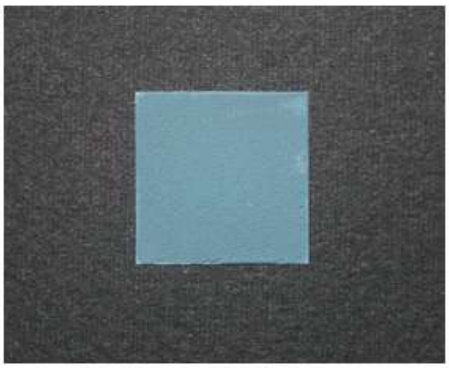

Figure 2-2. Optical photograph of membrane composed of silica particles with D_{ave} = 650 nm and CB.

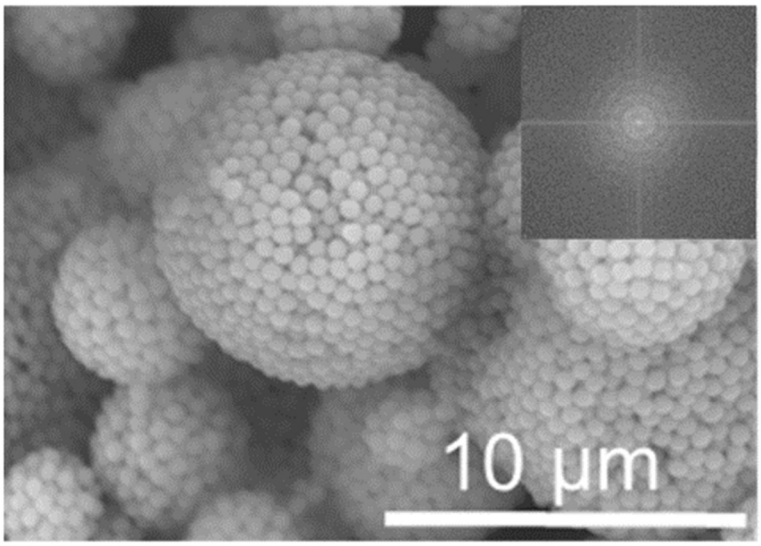

Figure 2-3. SEM image of secondary particles composed of silica particles with D_{ave} = 650 nm, Inset: two-dimensional Fourier power spectrum obtained from the SEM image.

2-3-3. Comparison of membranes composed of different silica particles and evaluation of the angle dependence of membranes composed of large silica particles (D = 650 nm)

To compare the newly obtained optical properties of the film comprising 650 nm fine silica particles with the above two kinds of samples, the scattering spectra of these films were measured using a scattering spectrum measuring apparatus with an integrating sphere (Figure 2-4). The peak appearing at the longest wavelength in each scattering spectrum is the first peak (☆), and the peak appearing at a shorter wavelength is the second peak (★), which has no angle dependence under irradiation with directional light. As the particle size increases, both the first peak and the second peak move to longer wavelengths. When the size of the fine silica particles is 280 nm, the position of the first peak is in the visible light region, but the position of the second peak is in the ultraviolet light region. When this film is regarded as a colored material, the second peak does not contribute to the color. However, in the scattering spectrum of the film composed of 650 nm fine silica particles, the position of the first peak is in the infrared light region, and the position of the second peak is in the visible light region. Judging from this result, if the diameter of the fine silica particles is 430 nm or greater, then the first peak is not observed in the visible light region. From this result, if the diameter of the fine silica particles is in the range of 430 to 725 nm, then the color mainly caused by the second peak from the colloidal amorphous array can be observed (see the inset of Figure 2-4).

From the angle dependence of the scattering spectra of the film composed of 650 nm fine silica particles, although the intensity of the peak changes with angle, the position of

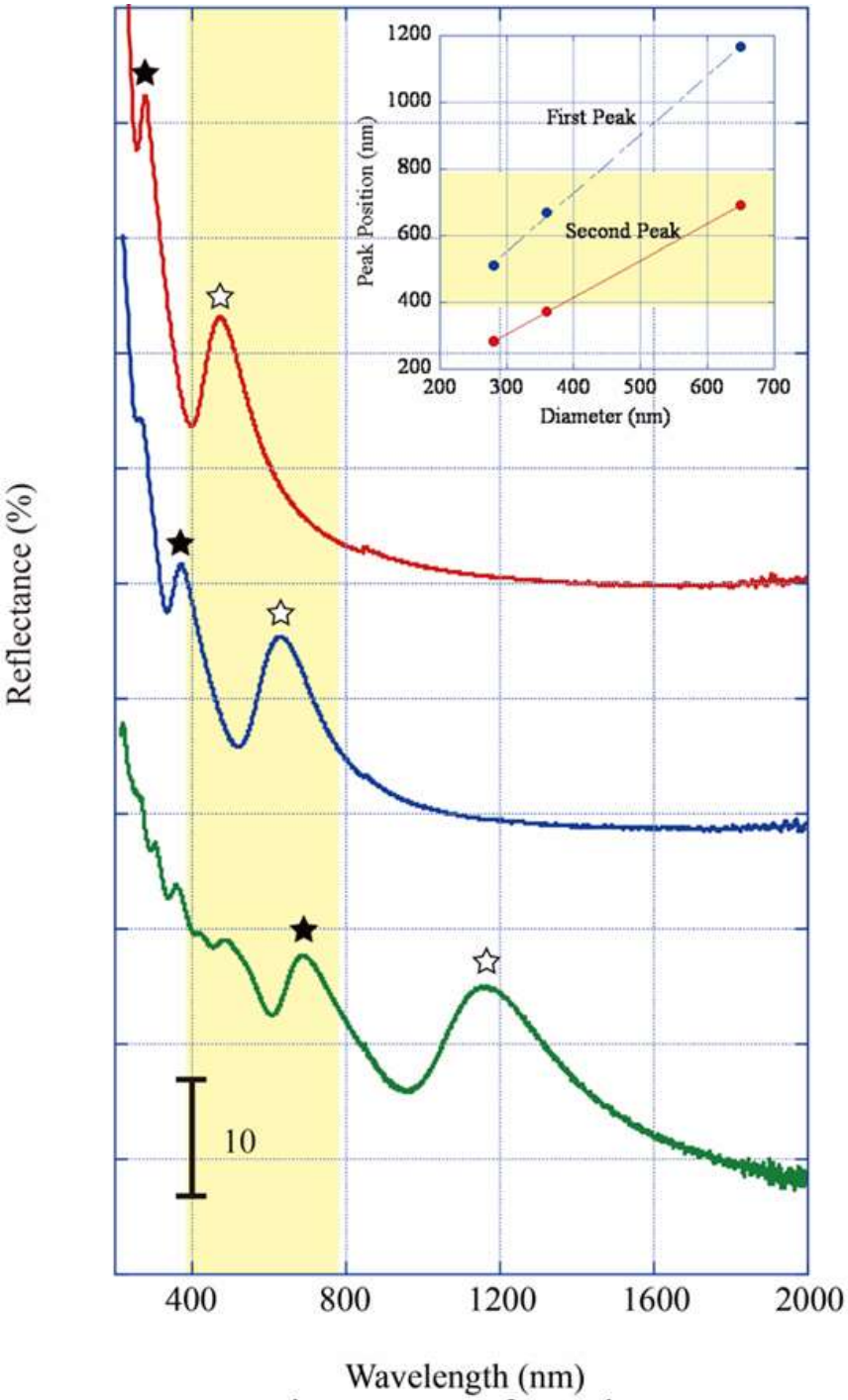

Figure 2-4. Scattering spectra of membrane composed of silica particles with D_{ave} = 280 nm(red), 360 nm(blue), and 650 nm(green). Inset: Plots of the positions of the first and the second peaks of the scattering spectra in Figure 4 versus the particle diameter.

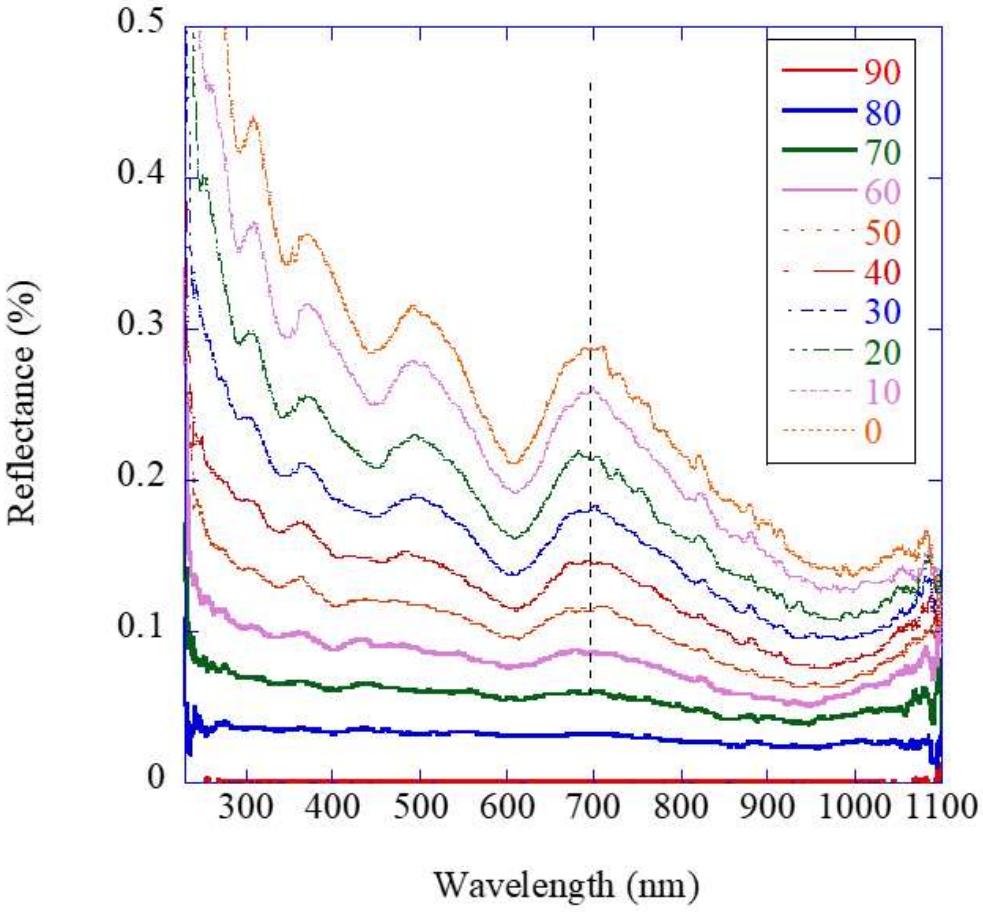

Figure 2-5. Angle-dependent scattering spectra of membrane composed of silica particles with D_{ave} = 650 nm and CB.

the peak does not change (Figure 2-5). In other words, as clarified using this second peak, a colored material with no angle dependence of the hue can be obtained.

In the inset of Figure 2-4, where the positions of the first peak and the second peak are plotted against the particle size, the particle size dependence of both peaks is proportional, but the slopes are different. This result suggests that the causes of the two scattering peaks are different. In this experiment, colloidal amorphous arrays were used to compare the coherent scattering generated from a colloidal amorphous array with the peak generated from Mie scattering occurring on the immediate shorter wavelength side.

2-4. Conclusion

By using the scattering generated by Mie scattering observed on the shorter wavelength side of the coherent scattering observed from a colloidal amorphous array, a colored material showing no angle dependence even under the condition of light irradiation from one direction could be produced. Since the position of this scattering peak linearly changes with the diameter of the fine silica particles, a colored material displaying an arbitrary color can be prepared by only changing the diameter of the fine silica particles to be used. Based on the obtained results, if materials exhibiting various colors without angle dependence can be obtained as stable structures using only inexpensive and safe materials, such as fine silica particles and CB, then a safe colored material could be obtained.

References

[1] M. Harun-Ur-Rashid, A. Bin. Imran, T. Seki, M. Ishi, H. Nakamura, Y. Takeoka,

ChemPhysChem, **11**, 579-583(2010).

[2] Y. Takeoka, M. Honda, T. Seki, M. Ishii, H. Nakamura, *ACS Appl. Mater. Interfaces,* **1**, 982-986(2009).

[3] J. D. Forster, H. Noh, S. F. Liew, V. Saranathan, C. F. Schreck, L. Yang, J. G. Park, R. O. Prum, S. G. J. Mochrie, C. S. O'Hern, H. Cao, E. R. Dufresne, *Adv. Mater.*, **22**, 2939-2944(2010).

[4] S. F. Liew, J. Foster, H. Noh, C. F. Schreck, V. Saranathan, X. Lu, L. Yang, R. O. Prum, C. S. O'Hern, E. R. Dufresne, H Cao, *Opt. Express*, **19**, 8208-8217(2011).

[5] Y. Takeoka, S. Yoshioka, A. Takano, S. Arai, N. Khamin, H. Nishihara, M. Teshima, Y. Ohtsuka, T. Seki, *Angew. Chem., Int. Ed.*, **52**, 7261-7265(2013).

[6] S. Yoshioka and Y. Takeoka, *ChemPhysChem*, **15**, 2209-2215 (2014).

[7] M. L. D. Marco, S. Semlali, B. A. Korgel, P. Barois, G. L. Drisko, C. Aymonier, *Angew. Chem., Int. Ed.*, **57**, 2-23(2018).

Chapter III

Characterization of Colloidal Amorphous Arrays Prepared by Uniaxial Pressure Application

3-1. Introduction

Mie scattering occurs for spherical particles. However, the light propagation varies with the particle size and refractive index[1,2].

In the case of a high refractive index particle, Mie resonance (other name: whispering gallery mode) occurs near the surface of the particle due to the enhanced light confinement effect[1,3,4]. High refractive index particles (e.g., titanium oxide and silicon) and micrometer-size particles are generally used to cause Mie resonance[5-13]. The reason why micrometer-size particles are used to cause strong resonance is because Mie resonance is a phenomenon similar to total reflection near the surface of the particle, and total reflection is difficult to achieve in nanometer-size particles having large curvature[2]. Mie resonance has been studied for application to lasers and resonators due to the ability to enhance the light confinement effect and light emission[1].

Here, in the case of low refractive index particles, such as silica and polystyrene nanometer-size particles, how does light propagate?

Researchers have divided opinions about this problem; however, Manoharan et al. argued that “Mie resonances” do not occur[14]. They argued that light reflected from the inner wall of a particle interfere in the particle similar to in thin film interference, and the

interfered light is scattered backward. They called this phenomenon “single particle scattering”.

In addition, they calculated the angle dependence of this scattering from an independent particle. They reported that the light scattering shows angle dependence when the viewing angle exceeds 60°. The effect that occurs when particles causing Mie scattering form aggregates has been studied by many researchers[5,6,9].

However, almost all researchers insist that aggregates do not participate in Mie scattering[14,15]. Therefore, the effect that occurs when particles causing Mie scattering form aggregates is unclear. We have to research this unclear point by using an experimental system and physical calculations.

In chapter II, angle-independent colored materials based on Mie scattering were prepared through the use of particles having a similar refractive index to the particles reported by Manoharan et al.[16].

When the viewing angle exceeds 60°, the Mie scattering peaks show angle independence.

Here, I questioned whether the effect for independent particles differs from that when particles causing Mie scattering form aggregates; as a result, angle-independent colored materials were prepared, and I began this research.

In chapter III, the experimental method for preparing samples is changed to enable the structure of the aggregates composed of particles causing Mie scattering to be defined.

In chapter II, membranes composed of secondary particles were prepared as colloidal amorphous arrays by the spray method[17]; however, how the particles packed, that is, the volume fraction, was difficult to define.

Several methods have been used to obtain colloidal amorphous arrays in air, including layer-by-layer methods[18], spin coating[19], and centrifugal precipitation[20]. However, these methods are not always easy, and the obtained samples are not easy to handle.

In chapter III, pellet-like colloidal amorphous arrays are prepared to easily define the volume fraction. The prepared pellets are free-standing samples, so they are easy to handle.

In this chapter, the scattering spectra derived from Mie scattering by pellet-like colloidal amorphous arrays and the calculated scattering spectra derived from Mie scattering by an independent single particle are compared.

As a result, the effect that occurs when the particles causing Mie scattering form aggregates is revealed.

In addition, I found that pellet-like colloidal amorphous arrays obtained by applying uniaxial pressure have anisotropy in the particle arrangement, and the angle dependence of the structural color is decreased.

3-2. Experimental section

3-2-1. Materials

Monodisperse fine silica particles (2.3 g/cm^3) with average diameters of 197, 260, 300, 350, 395 and 502 nm were purchased from Fuji Chemical Co., Ltd. for use in this study. CB (average diameter of primary particles: 28 nm) provided by Tokai Carbon Co., Ltd. was used in this study.

3-2-2. Preparation of pellets consisting of fine silica particles

First, to make the particle size uniform, the fine silica particle powder was pulverized for 120 seconds using a commercial pulverizer (sanitary crusher made by Mitaka Industries, SC-02). As a result, secondary particles with an average diameter of 9 μm were obtained. An under punch and a spacer were attached to a die with a 10 mm diameter cylindrical hole, a predetermined amount of pulverized powder was placed in this cylindrical hole, and vibration filling was performed. Pellet molding was carried out by compression with a force of 50 kN using a powder-molding machine (Mighty Press MT-50H) (Figure 3-1(a)). From the volume and weight of the obtained pellets, the filling ratio of the particles in the pellets was determine using the density of the fine silica particles.

3-2-3. Scattering spectrum measurements

The angle dependence of the scattering spectrum was determined by means of a UV-vis spectrometer (Nippon Bunko Company, V-670) and a goniometer (ARMN-735). A pellet was placed on a holder prepared by processing a plastic plate and subsequently measured. The light was incident from a direction perpendicular to the flat surface or side of the pellet, the detector was placed at various angular positions relative to the incident direction, and the scattering spectrum was measured (Figure 3-2).

3-2-4. Observation of electron microscope images

The arrangements of the fine silica particles in the arrays were investigated by scanning electron microscopy (SEM, Hitachi, MiniScope TM3000). These samples were coated

with a 10-nm Pt layer using a magnetron sputtering apparatus (MSP-1S), and images were obtained using a scanning electron microscope operated at 15 kV. A two-dimensional fast Fourier transform was performed on the measured images using ImageJ to evaluate the particle arrangement.

3-2-5. Optical pictures obtained with a digital camera

Photographs revealing the structural colors of the samples were taken with a digital camera.

3-3. Results and discussion

3-3-1. Preparation of colloidal amorphous arrays as pellets

In this study, colloidal amorphous arrays formed from fine silica particles were prepared by compressing powdery fine silica particles in a uniaxial direction and processing the compressed powder into disk-shaped pellets. Since commercially available powdery fine silica particles form large agglomerates, making the agglomerates as fine as possible is better for forming disk-shaped pellets with a uniform packing density from colloidal amorphous arrays. Thus, prior to preparing the pellets, the agglomerates of fine silica particles were ground with a granulator. When packing and compacting finely divided powdery fine silica particles in the mold, the pellet was molded under appropriate pressure conditions using a powder-molding machine (Figure 3-1(a)) so that the pressure on the powder was evenly applied to the top and bottom (Figure 3-1(b)). Pressurization was performed at 50 kN for 2 to 10 min during pellet preparation. In each system of fine

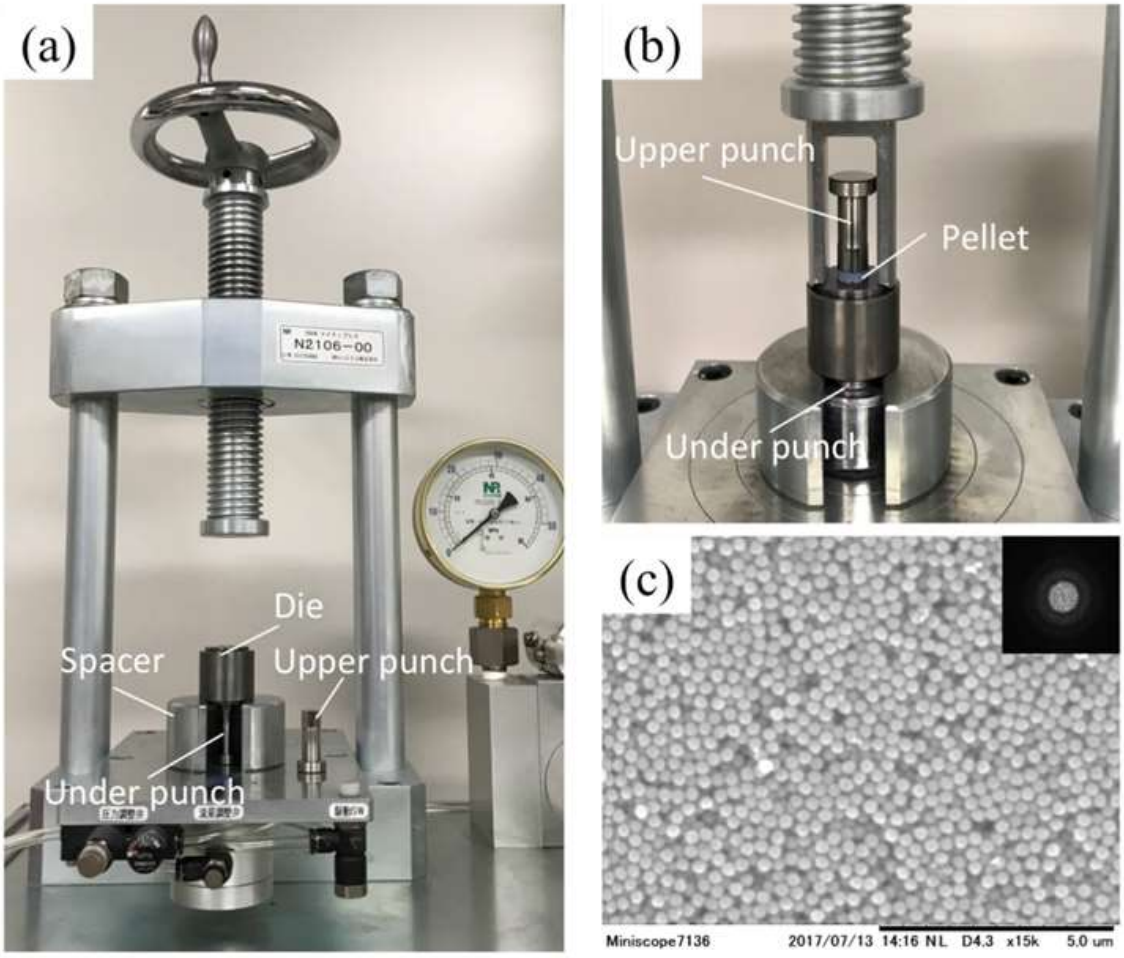

Figure. 3-1 (a) A photograph of a pellet former used to make a pellet-like colloidal amorphous array. (b) A photograph immediately after molding a pellet composed of fine silica particles and carbon black prepared using the pellet former in (a). (c) Electron micrograph and its Fourier transform image of the surface of a pellet prepared from fine silica particles with a particle size of 197 nm and 0.5 wt% carbon black.

silica particles with different diameters, disk-shaped pellets were prepared with an average filling rate of 54 vol%, a diameter of 10 mm, and a thickness of approximately 3 mm. This filling rate is consistent with the density of the random densest packing in which the monodisperse spheres are most loosely packed. Compared with the theoretical non-normal filling rate (63.4%), the filling ratio of the particles in the obtained pellet is low. However, if the pellet is molded under higher pressure, then the fine silica particles may be broken. An electron micrograph of the flat surface of a pellet obtained by this method and its Fourier transform image show that the fine silica particles with uniform diameters are arranged in a state with short-range order (Figure 3-1(c)). In addition, since the colloidal amorphous array produces multiple scattering of light inside it, the pellets were prepared with 0.5 wt% CB mixed in the fine silica particles to reduce the multiple scattering of light.

3-3-2. Optical properties of colloidal amorphous arrays composed of particles causing Mie scattering

Pellets composed of fine silica particles with large sizes were prepared such that the scattering peak occurred in the visible light region. Figures 3-2(a), 3-2(b) and 3-2(c) show the angle dependence of the scattering spectra of the pellet-like colloidal amorphous arrays consisting of fine silica particles with sizes of 350 nm, 395 nm and 502 nm, respectively. These pellets were also prepared in a state where 0.5 wt% CB was mixed with the fine silica particles to reduce the multiple scattering of light. In the system with 350 nm particles, since a scattering peak derived from the short-range order is observed

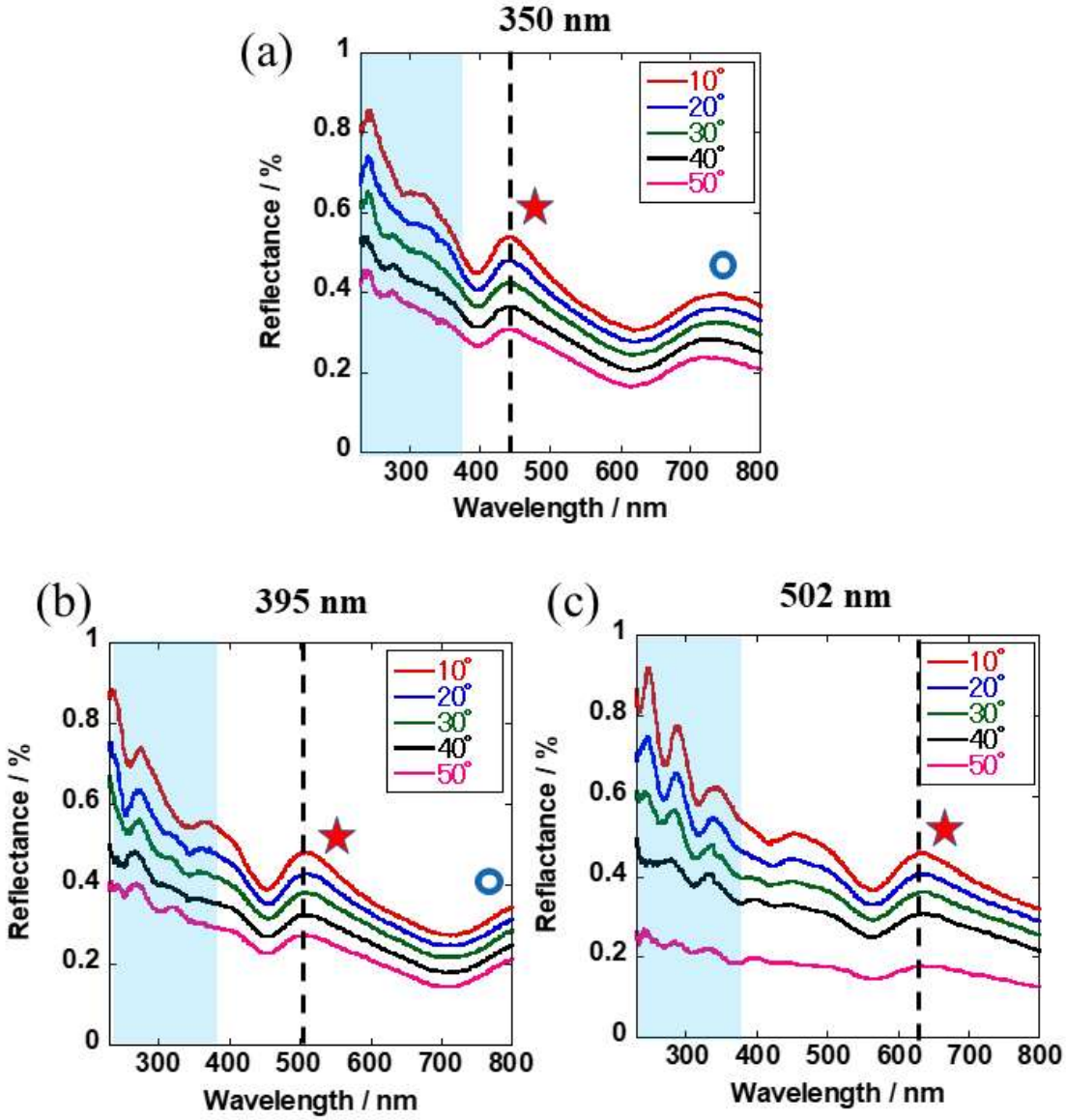

Figure 3-2. (a) Angular dependence of the scattering spectra observed from the compression direction of a pellet consisting of 0.5 wt% carbon black and fine silica particles with a particle size of 350 nm. (b) Angular dependence of the scattering spectra observed from the compression direction of a pellet consisting of 0.5 wt% carbon black and fine silica particles with a particle diameter of 395 nm. (c) Angular dependence of the scattering spectra observed from the compression direction of a pellet consisting of 0.5 wt% carbon black and fine silica particles with a particle size of 502 nm.

at approximately 740 nm, red light is scattered according to this scattering peak. However, a larger scattering peak without angle dependence involving Mie scattering occurs at 440 nm. As a result, a blue color is observed for the pellet formed of fine particles with a size of 350 nm. Furthermore, if fine silica particles with a larger size are used, then the associated Mie scattering peak shifts to a longer wavelength, and the scattering peak derived from the short-range order does not occur in the visible region (Figures 3-2(b) and 3-2(c)).

Pale blue, pale green and pale red colors were observed for the pellets composed of fine silica particles with sizes of 197 nm, 260 nm and 300 nm, respectively, mixed with 0.5 wt% CB (Figures 3-2(a), 3-2(b), and 3-2(c)). Similarly, pale blue, pale green, and pale red were also observed for the pellets composed of particles with larger diameters of 350 nm, 395 nm, and 502 nm, respectively, mixed with 0.5 wt% CB (Figure 3-3(a)). By increasing the amount of incorporated CB, more saturated colors can be observed for these pellets. This increased saturation occurs because the scattering intensity is suppressed and the scattering peak becomes prominent due to the reduction in the multiple scattering occurring inside the colloidal amorphous array (Figures 3-3(b)-5(d)). The short-range order-derived peak deviates from the visible light region when the size of the fine silica particles is 350 nm or greater (peak 1 in Figure 3-3(e)). The Mie scattering peak occurring on the short wavelength side appears in the visible light region when the diameter of the fine silica particles is 300 nm to 620 nm (peak 2 in Figure 3-3(e)). From the results presented above, if pellets composed of fine silica particles of 350 nm to 620 nm are used, then colors with no angle dependence are exhibited by utilizing the scattering

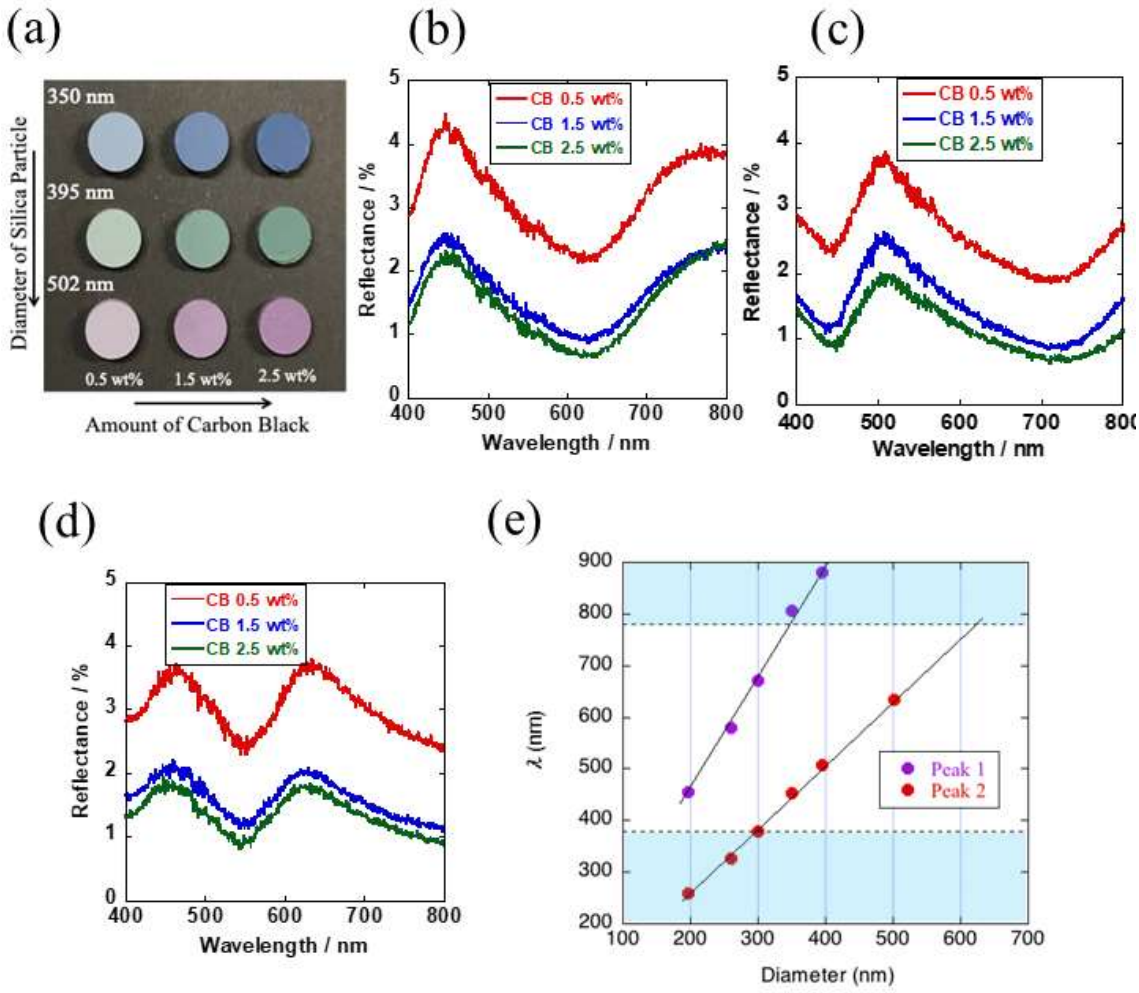

Figure. 3-3 (a) Photograph of pellets prepared by mixing 0.5-2.5 wt% carbon black and fine silica particles with average particle diameters of 350 nm, 395 nm, and 502 nm. (b) Scattering spectra of the pellet with an average particle size of 350 nm shown in (d). (c) Scattering spectra of the pellet with an average particle diameter of 395 nm shown in (a). (d) Scattering spectra of the pellet with an average particle size of 502 nm shown in (a). (e) A diagram in which the position of the scattering peak derived from the short-range order obtained from the scattering spectra of the pellets composed of fine silica particles of each particle size and the peak derived from Mie scattering observed on the short wavelength side is plotted against each particle size.

peak derived from Mie scattering, which occurs immediately on the short wavelength side of the peak derived from the short-range order.

3-3-3. Comparison of Mie scattering from colloidal amorphous arrays and single particles

Figure 3-4(a) shows the scattering spectra observed for pellets of fine silica particles with diameters ranging from 197 nm to 502 nm. Light is irradiated from the compression direction of pellet, and a detector is oriented 10° from the light irradiation direction to measure the scattering spectra. In the figure, the horizontal axis is x ($x=D\pi/\lambda$), and the vertical axis is the light reflectance. Here, D is the diameter of the fine silica particles, and λ is the wavelength of light. Figure 3-4(b) shows the theoretically calculated scattering intensities for Mie scattering. The vibration in the spectrum is roughly reproduced, which supports the assertion that the peak on the short wavelength side originates from Mie scattering. The scattering peak indicated by the blue circle, which is located at x = 1.45 in Figure 3-4(a), is thought to originate from the short-range order, as discussed above. Interestingly, in the spectrum from Mie theory, another peak is located at a position near this peak. Thus, although the wavelength shift of the peak indicated by the blue circle suggests that its origin is the interference due to the short-range order (structural factor), the scattering efficiency is enhanced by the Mie scattering (form factor). Careful comparisons between the experimental and theoretical spectra reveal many differences, e.g., in the peak positions, heights, and shapes. These differences mainly exist because the colloidal amorphous arrays in the pellet form a short-range

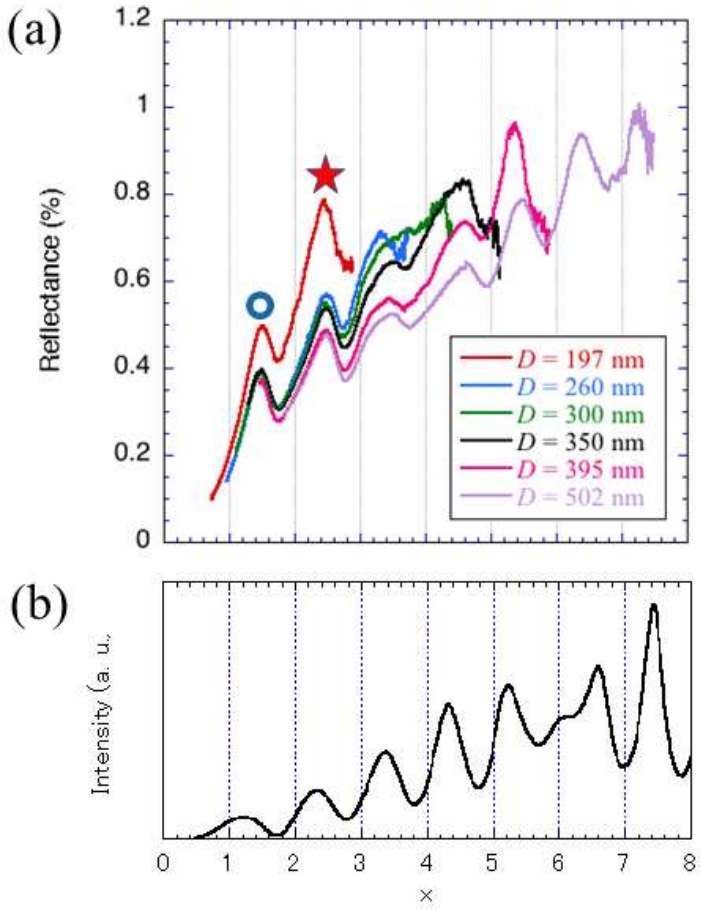

Figure. 3-4 (a) Light is irradiated from the compression direction of the pellet composed of fine silica particles with different particle sizes, and the scatter spectra observed at an angle of 10 ° from the light irradiation direction is plotted with x (x=Dπ/λ) as the horizontal axis. (b) Theoretically calculated scattering spectrum in the Mie theory. The scattering angle is 10 ° , which is 170 ° from the direction of the incident light. The diameter of the particle is assumed to be 300 nm with a refractive index of 1.47. The surrounding medium is air. The spectrum is averaged for two polarizations.

ordered aggregate with single spherical particles in contact with each other, which is a different situation from the single scattering sphere assumed in Mie theory. For example, as x increases, the scattering intensity increases, but the height of the peak is not as expected in the theory. This behavior seems to be related to the fact that CB absorbs light more efficiently on the short wavelength side.

3-3-4. Optical properties of colloidal amorphous arrays obtained by uniaxial pressure application

To characterize the optical properties of the amorphous arrays, we measured the angle-dependent scattering spectra (Figure 3-5). Figure 3-5(a) shows the results for the sample with a particle diameter of D = 300 nm. The spectra were measured for the pellet surface on which the pressure was applied. The incident light was normal to the surface, whereas the detector was placed at a 10-50° angle with respect to the incident direction. Each spectrum shows peaks at approximately 636, 380, and 280 nm. The two peaks on the short wavelength side seem to be approximately angle independent. However, the peak appearing at the longest wavelength exhibits a blueshift as the observation angle increases; the position of this peak at the observation angle of 10° is 636 nm, and when the observation angle is changed to 50°, the peak shifts to 623 nm. Such angle dependence originates from the coherent scattering due to the short-range order of the colloidal amorphous arrays[21]. Because the interference condition includes the angle as a parameter, the color of the colloidal amorphous array changes for different observation directions under directional light illumination. However, the pellet-like colloidal amorphous arrays

exhibit iridescence smaller than that of the colloidal amorphous arrays prepared by conventional methods. Figure 3-5(c) shows the angle dependence of the peak wavelengths (these values are normalized by dividing by the peak wavelength at 10°). The peak shift is very small: the peak shift is only approximately 2% at 50°. For a sample prepared by a different method, that is, the colloidal amorphous array consisting of secondary particles prepared by the spray method, when the observation angle is 50°, the peak position is shifted by 6% to a shorter wavelength based on the wavelength of the scattering peak observed at 10°[17]. The angle dependence of the sample in the present study is suppressed to one-third that of the sample in the abovementioned study. The cause of this suppression of the angle dependence is considered to be related to the anisotropic nature of the sample because the sample is produced under uniaxial stress. To confirm this assertion, a measurement was performed on the side of the sample (Figure 3-5(b)). In the scattering spectrum at 10°, the scattering peak from the short-range order appears at 699 nm, which is approximately 10% longer than the measurement result (636 nm) from the compression surface. Additionally, when the observation angle is changed to 50°, the scattering peak shifts to 658 nm. This amount of peak shift is approximately 6%, as shown in Figure 3-5(c). These results suggest that in the pellet, anisotropy exists in the length of the short-range order of the fine silica particle aggregates; we believe that the particles are densely packed in the compression direction and sparsely packed in the perpendicular direction.

Similar effects were also observed in pellets made of fine silica particles of different sizes. Figure 3-6 shows that in the pellets formed from fine silica particles with an average

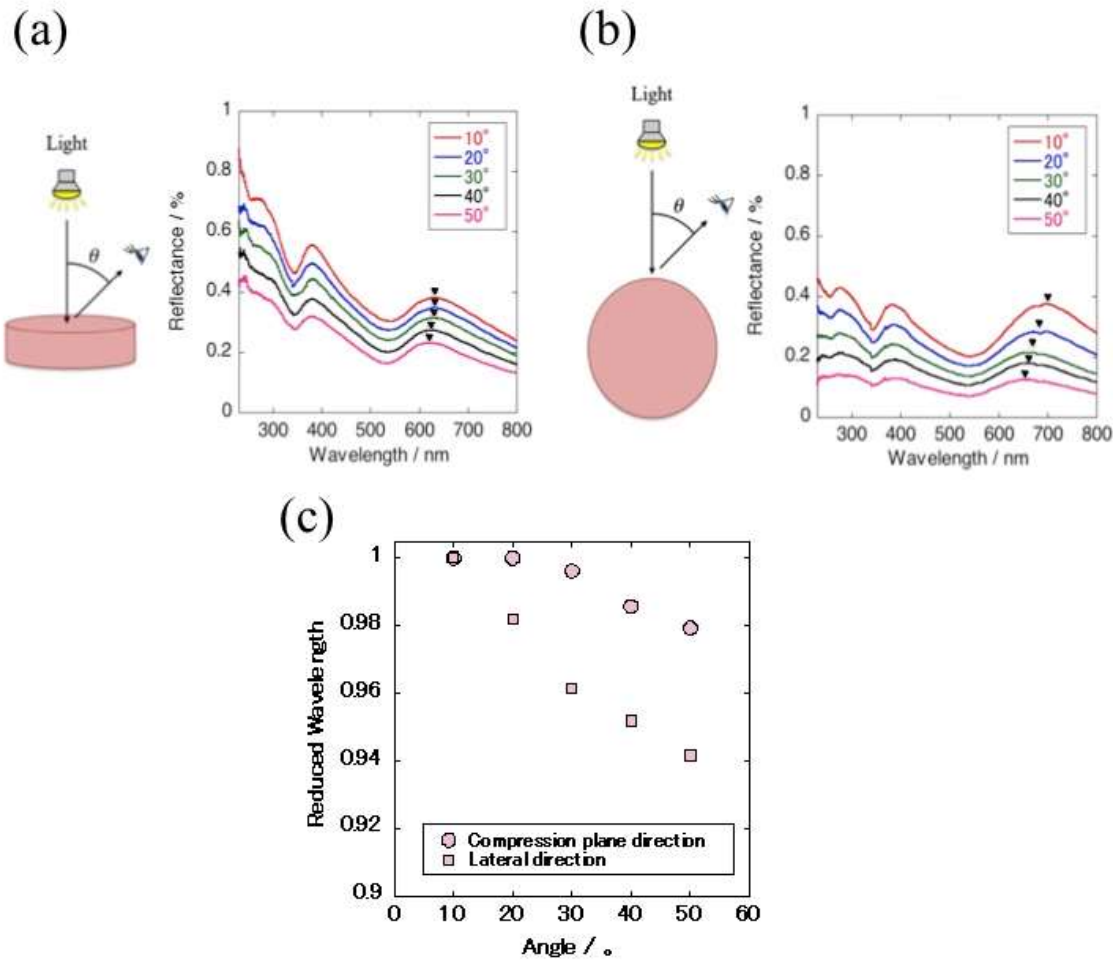

Figure. 3-5 (a) A conceptual diagram for measuring the angular dependence of the scattering spectrum by irradiating light from the compression direction of the pellet and the angular dependence of the scattering spectrum actually obtained. (b) A conceptual diagram for measuring the angular dependence of the scattering spectrum by irradiating light from the direction perpendicular to the compression direction of the pellet and the angular dependence of the scattering spectrum actually obtained. (c) Angular dependence of the scattering peak wavelength derived from the short-range order according to the scattering spectra shown in (a) and (b). With the scattering peak wavelength obtained at an observation angle of 10 ° as a reference value, the value obtained by dividing the wavelength of the scattering peak observed at other angles by the scattering peak wavelength of 10 ° is taken as the "reduced wavelength".

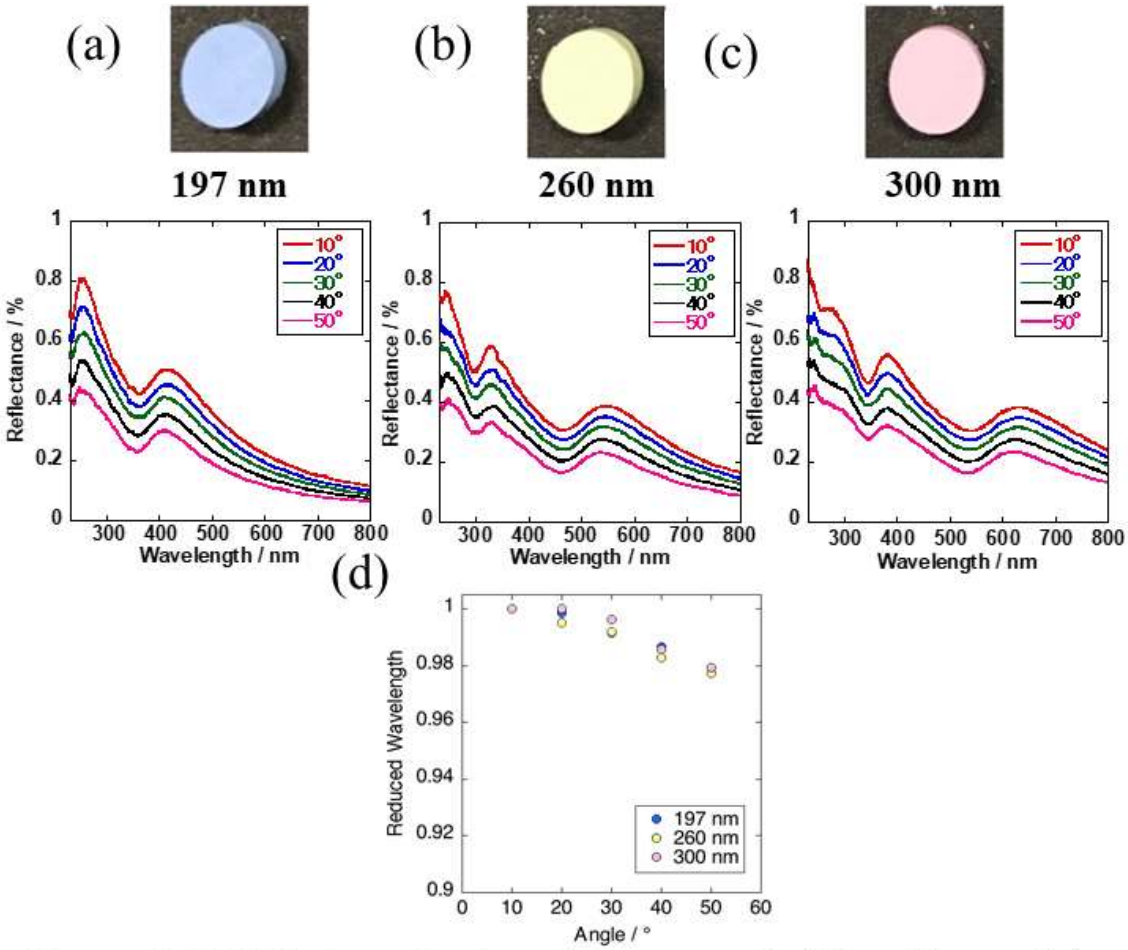

Figure. 3-6 (a) Photograph of a pellet composed of fine silica particles with a particle diameter of 197 nm and 0.5 wt% carbon black (relative to the fine silica particle weight) and the angular dependence of the scattering spectra observed from the compression direction. (b) Photograph of a pellet composed of fine silica particles with a particle diameter of 260 nm and 0.5 wt% carbon black and the angular dependence of the scattering spectra observed from the compression direction. (c) Photograph of a pellet composed of fine silica particles with a particle size of 300 nm and 0.5 wt% carbon black and the angular dependence of the scattering spectra observed from the compression direction. The scatter spectra of Figure 3c are the same as the scatter spectra results shown in Figure 2a. The white parts of (a) through (c) indicate the visible light region. (d) Angular dependence of the scattering peak wavelength derived from the short-range order obtained from the scattering spectra of (a) through (c).

diameter of 197 nm, 260 nm, and 300 nm, when observed at 10°, the scattering peaks derived from the short-range order occur at 421 nm, 552 nm, and 636 nm, respectively. However, as shown in Figure 3-6(d), the angle dependence of the coherent scattering observed from the compression surface is as small as 2%. These results show that the pressure-induced preparation method results in a colloidal amorphous array that has a smaller iridescence than the colloidal amorphous arrays produced by other methods, such as the spray method.

3-4. Conclusion

A method that utilizes uniaxial pressure application was used to make colloidal amorphous arrays. A sample with a small iridescence was obtained despite the coherent scattering due to the short-range order. This behavior is suggested to be caused by the anisotropic nature of the sample. Moreover, numerous scattering peaks with nearly no angle dependence were observed on the short wavelength side. These peaks were considered to originate from Mie scattering. When a particle with a large size is used, a material exhibiting this scattering peak as the main coloration source can be obtained, making it possible to obtain a colorant with no angular change. The method of applying uniaxial pressure is expected to become a simple method for easily forming a pellet-like colored material by improving the conditions during pressure application and the feeding method in the future.

References

[1] F. Vollmer and S. Arnold, *Nat.method*, **5**, 591-596 (2008).

[2] H.C. Van de Hulst, "Light scattering by small particle", Dover Publication, Inc., New York, p151.

[3] Y. Yamamoto and R. E. Slusher: *Phys. Today* Junuary, 66 (1993).

[4] R. K. Chang and A. J. Campillo. ed.: Optical processes in microcavitites (World Scientific Publishing, Singapore, New Jersey, London, Hong Kong, 1996).

[5] D. Montesdeoca; F. Bayat; A. Espinha; A. Blanco; C. Pecharroman; C. Lopez, *Part Part Syst Char*., **33** (12), 871-877(2016).

[6] L. Shi, J. T. Harris, R. Fenollosa, I. Rodriguez, X. Lu, B. A. Korgel and F. Meseguer, *Nat.Commun*., **4**, 1-7 (2013).

[7] M. Naffouti, T. David, A. Benkouider, L Favre, A. Ronda, I. Berbezier, S. Bidault, N. Bonodd and M. Abbarchi, *Nanoscale*, **8**, 2844-2849 (2016).

[8] J. Zhou, A. Panday, Y. Xu, X. Chen, L. Chen, C. Ji, L. J. Guo, *Phys. Rev. Lett.*, **120**, 253902 (2018).

[9] K. Yoshihara, M. Sakamoto, H. Tamamitsu, M. Arakawa, K. Saitow, *Adv. Opt. Mater.*, **6**, 1800462 (2018).

[10] M. L. D. Marco, S. Semlali, B. A. Korgel, P. Barois, G. L. Drisko, C. Aymonier, *Angew. Chem., Int. Ed.*, **57**, 2-23 (2018).

[11] S. Kushida, D. Okada, F. Sasaki, Z-H. Lin, J-S. Huang, Y. Yamamoto, *Adv. Opt. Mater.*, **5**, 1700123 (2017).

[12] T. A. Kumara, M. A. Mohiddon, N. Dutta, Nirmal K. Viswanathan, and S. Dhara, *Appl. Phys. Lett.*, **106**, 0511101 (2015).

[13] D.S. Weiss, V. Sandoghdar, J. Hare, V. Lefevre-Seguin, J.-M. Raimond, and Haroche,

Optics Letter, 20, 1835-1837 (1995).

[14] S. Magkiriadou, J-G. Park, Y-S. Kim, and V. N. Manoharan, *Phys. Rev. E.*, **90** (6) (2014).

[15] S-H. Kim, V. Hwang, S. G. Lee, J-W. Ha, V. N. Manoharan, and G-R. Yi, *Small*, **15**, 1900931 (2019).

[16] Y. Naoi, T. Seki, S. Yoshioka, Y. Takeoka, *Mol. Cryst. Liq. Cryst*., **688**, 105-113 (2019).

[17] Y. Takeoka, S. Yoshioka, A. Takano, S. Arai, N. Khamin, H. Nishihara, M. Teshima, Y. Ohtsuka, T. Seki, *Angew. Chem. Int. Ed.*, **52**, 7261-7265(2013).

[18] D. T. Ge; L. L. Yang.; G. X. Wu; S. Yang, *J. Mater. Chem. C*, **2** (22), 4395-4400(2014).

[19] M. Iwata.; M. Teshima.; T. Seki; S. Yoshioka; Y. Takeoka, *Adv. Mater.*, **29** (26)(2017).

[20] K. Katagiri; Y. Tanaka; K. Uemura.; K. Inumaru; T. Seki; Y. Takeoka, *Npg. Asia. Mater.*, **9**. 28, (2017).

[21] S. Yoshioka and Y. Takeoka, *ChemPhysChem*, **15**, 2209-2215(2014).

Chapter IV

Angle-Independent Colored Materials with Mie Scattering and Rayleigh Scattering in Response to Pressure

4-1. Introduction

For light scattering from an independent single particle, such as Rayleigh scattering and Mie scattering, the approximate solution and the exact solution were obtained in the distant past.

However, Rayleigh scattering technology is still out of reach due to its properties. Their practical use has not been realized despite the well-known phenomena. Rayleigh scattering is light scattering that occurs when the particle size is smaller than the light wavelength[1,3]. The reflectance of scattered light is inversely proportional to the fourth power of the light wavelength. Therefore, shorter wavelength light is reflected. Light scattered by Rayleigh scattering is scattered not only in the anterior direction but also backward, and the color shows low angle dependence. However, the reflectance of longer wavelength light is low. Therefore, changing the hue of colored materials by using Rayleigh scattering is difficult. This is the reason why colored materials based on Rayleigh scattering have not been researched.

In contrast, for Mie scattering, the wavelength of the scattered light changes with the particle size[4-8]. Therefore, Mie scattering can be used for colored materials because changing the hue is easy. Mie scattering has been studied for application purposes; however, this research has a short history.

Recently, Manoharan et al. reported materials that can switch from Rayleigh scattering to Mie scattering in response to temperature[9]. They prepared PS/PNIPAM core-shell particles. Switching from Rayleigh scattering to Mie scattering was achieved by using the PNIPAM properties of shrinking and becoming opaque at high temperature.

In this research, I was inspired by their paper, and I planned to investigate angle-independent colored materials that change from Mie scattering to Rayleigh scattering in response to external stimuli.

Colored materials with a certain response to external stimuli are expected to be applicable to sensors[10,11]. Gong and Fudouzi reported sensors with a response to pressure by using colloidal crystals[12,13]. Our group also reported sensors with a response to temperature by using colloidal amorphous arrays[14].

However, the angle dependence of sensors using the response to external stimuli of the structural color is sometimes problematic because we cannot judge the change in the external environment when the hue changes with the viewing angle.

In chapter III, the angle independence of the color for aggregates composed of particles causing Mie scattering was proven. In this chapter, I prepare colored materials that change their hue in response to pressure by combining aggregates causing Mie scattering and Rayleigh scattering showing angle independence.

The design of colored materials based on Rayleigh scattering showing low angle dependence increases the breadth of application of this scattering. Therefore, the design of materials causing this scattering was selected. First, non-crosslinked PMMA particles were selected because their shape can be changed by pressure due to their softness. The

particle size of PMMA was selected to be approximately 400 nm and 350 nm to cause Mie scattering. In addition, the condition that nanometer-size scatterers were uniformly dispersed was essential to visualize the color caused by Rayleigh scattering. Therefore, I expected that particles causing Rayleigh scattering would be uniformly dispersed by forming aggregates of PMMA/TiO_2 core-shell particles (Figure 4-1(a)).

Moreover, when aggregates of PMMA particles were pressed, extinction of Mie scattering and occurrence of Rayleigh scattering caused by the air gaps of the pressed aggregates were expected. I also expected that the light would be strongly scattered by Mie scattering when using high refractive index particles, and the reflectance from Rayleigh scattering would be increased because the Rayleigh scattering from air gaps would contribute to the light scattering from titanium oxide particles (Figure 4-1(b)).

In this chapter, I thus report angle-independent colored materials with changing hue in response to pressure because of a phenomenon change from Mie scattering to Rayleigh scattering.

4-2. Experimental section

4-2-1. Materials

PMMA particles with an average size of 400 nm (MP1000) and 350 nm (MP2200) were purchased from Souken Chemical Co., Ltd. for use in this study.

Titania oxide particles with an average size of 7 nm in a HCl water suspension (30 wt%) (STS-02) were purchased from Ishihara Sangyo Co., Ltd. for use in this study.

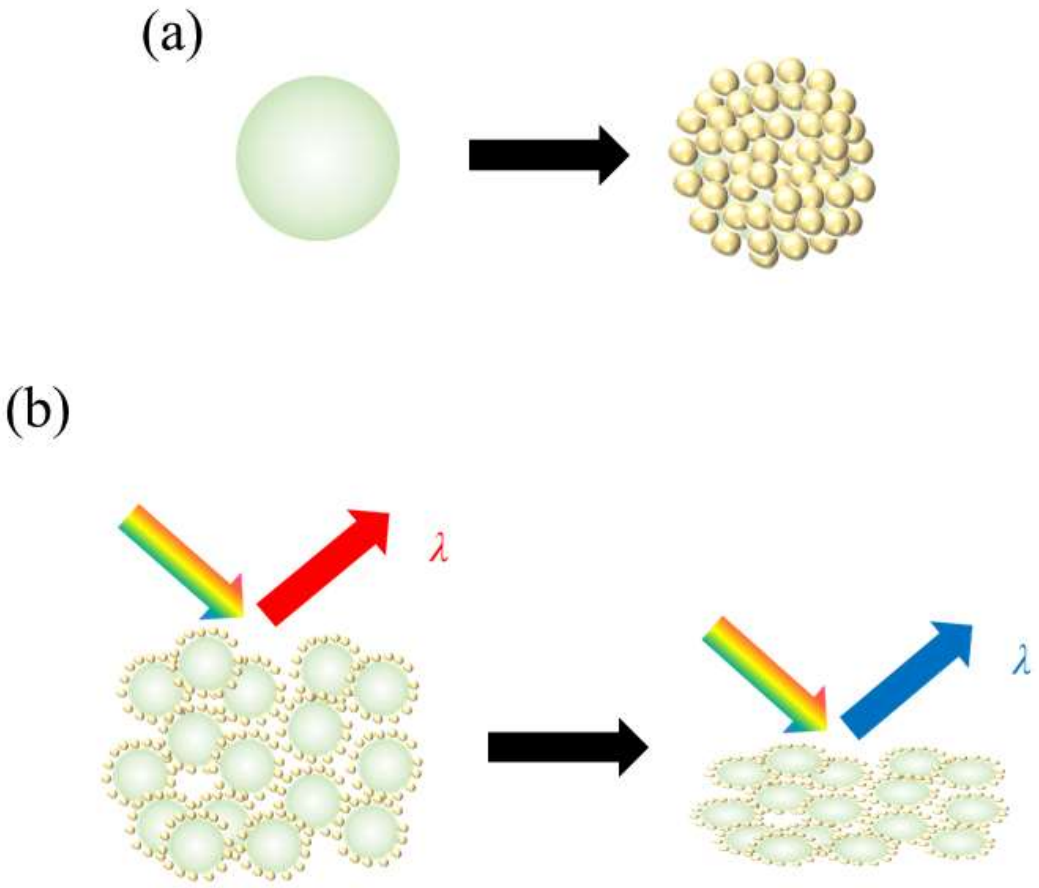

Figure 4-1. (a) A scheme of PMMA/TiO_2 particle. (b) A scheme of evaluating optical property of an aggregate composed of PMMA/ TiO_2 particles.

4-2-2. Preparation of PMMA/TiO_2 core-shell particles

PMMA particles (5 g) were added to TiO_2 HClaq (10 g). Pure water (40 g) was mixed with the prepared suspension and stirred for 2 hours at room temperature.

The mixture was centrifuged (1700 rpm) for 5 min. The supernatant liquids were removed. The remaining particles were dispersed in pure water. These procedures were repeated 4 times.

Washed particles were redispersed in pure water. A water suspension of CB particles (19.2 wt%, 5.5 μl) was added to the prepared suspension of PMMA/TiO_2 particles. The mixture was freeze dried.

4-2-3. Preparation of pellets composed of PMMA/TiO_2 particles

Pellet molding was carried out by compressing PMMA/TiO_2 particles (0.25 g) with a force from 10 kN to 50 kN using a powder-molding machine (Mighty Press MT-50H), as described in chapter III.

4-2-4. Scattering spectrum measurements

The angle dependence of the scattering spectrum was determined by means of a UV-vis spectrometer (Nippon Bunko Company, V-670) and a goniometer (ARMN-735). An aggregate was placed on a holder prepared by processing a plastic plate and subsequently measured. The light was incident from a direction perpendicular to the flat surface of the aggregate, the detector was placed at various angular positions relative to the incident direction, and the scattering spectrum was measured.

4-2-5. Observation of electron microscope images

PMMA/TiO_2 core-shell particles and pellets were observed by using a scanning electron microscope (JEOL, JSM-7500FA).

Samples were coated with a 5 nm osmium layer using a magnetron sputtering apparatus, and the images were acquired using SEM operated at 15 kV by using an osmium plasma coater (Filgen, OPC60A).

An electron micrograph of a pellet composed of PMMA particles was obtained by SEM (Hitachi, MiniScope TM3000).

These samples were coated with a 10-nm Pt layer using a magnetron sputtering apparatus (MSP-1S), and images were obtained using a scanning electron microscope operated at 15 kV. A two-dimensional fast Fourier transform was performed on the measured images using ImageJ to evaluate the particle arrangement.

4-2-6. Observation of the cross-section of pellets

Pellets were embedded in epoxy resin (Quetol-812, DDSA, MNA, DMP-30, Nisshin EM CO.), which was cut to obtain cross-sections of pellets for observation by SEM.

4-2-7. Optical pictures obtained with a digital camera

Photographs of prepared composite particles and pellets were taken with an iPhone 6s.

4-2-8. EDX analysis of a surface composed of PMMA/TiO_2 particles

Elemental analysis of titanium was performed on the surface of a pellet composed of PMMA/TiO_2 particles using a MiniScope TM3000 with a SwiftED 3000 energy dispersive X-ray spectrometer (Hitachi).

4-3. Results and discussion

4-3-1. Observation of prepared PMMA/TiO_2 particles

Some methods to prepare core-shell particles with TiO_2 shells have been reported, such as the sol-gel reaction[15-18].

In this research, heteroaggregation was used to easily prepare core-shell particles[19]. Heteroaggregation is a method for preparing composite particles using the electrostatic interaction of particles[20]. The PMMA particles (MP1000 and MP2200) used in this experiment have a negative charge. Anatase-type titanium oxide has a positive charge in acid solution at pH 6. Therefore, PMMA particles were added to an acid suspension of titanium oxide particles. Finally, PMMA/TiO_2 core-shell particles were prepared.

Figure 4-2 shows an electron micrograph of the prepared PMMA/TiO_2 particles. PMMA/TiO_2 particles were obtained as raspberry-like particles.

4-3-2. Optical properties of PMMA/TiO_2 particles

To evaluate the optical properties of the prepared core-shell particles, photographs were taken, and spectra were measured. Core-shell particles were placed on tape, and the spectra were measured in the same way as in chapters II and III. A comparison of PMMA particles and PMMA/TiO_2 particles containing CB particles is shown in Figure 4-3 and

(a)

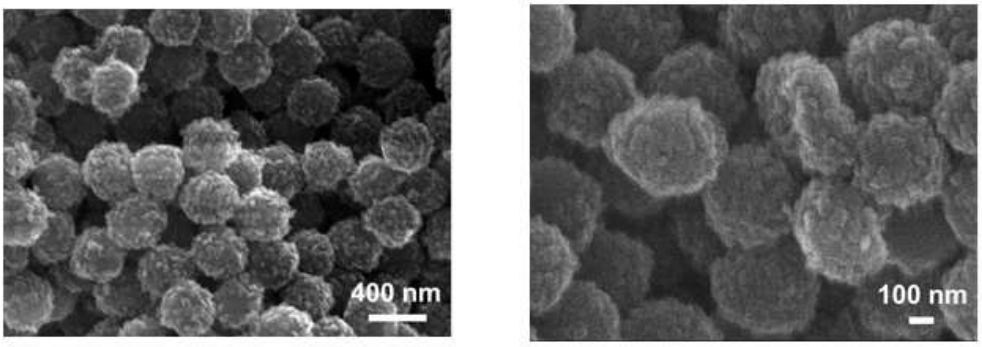

(b)

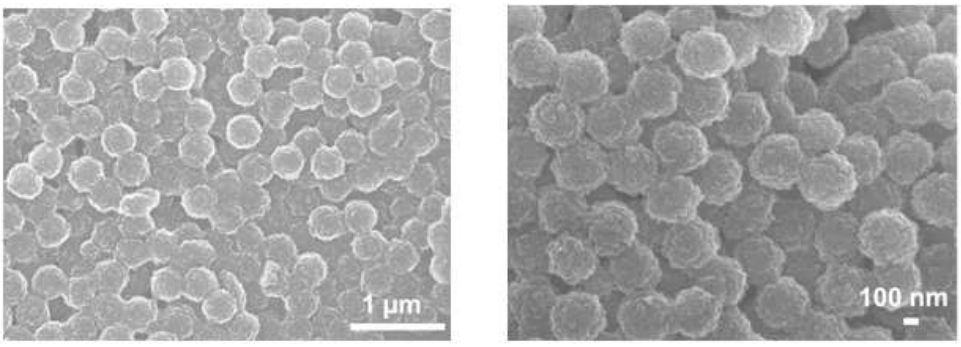

Figure 4-2. Electron micrograph of PMMA/TiO_2 particles. (a) PMMA/TiO_2 particles using PMMA particles with particle size of average 400 nm. (b) PMMA/TiO_2 particles using PMMA particles with particle size of average 350 nm.

Figure 4-4. Figure 4-3 and Figure 4-4 shows the result using PMMA particles with size of average 400 nm (MP1000) and average 350 nm (MP2200), respectively.

In the spectra of PMMA particles (average size = 400 nm), a scattering peak from Mie scattering is observed at 590 nm. After coating with titanium oxide particles, the scattering peak shifts to a longer wavelength because the particle size is larger and the refractive index is higher.

In Figure 4-3(b), the baseline is increased; in other words, the effect from multiple scattering is increased compared to that before coating despite the CB particles. The reason is that multiple scattering occurs between the titanium oxide particles.

The spectra using PMMA particles with particle size of average 350 nm exhibited similar results. In Figure 4-4 (a), PMMA particles (average size = 350 nm), a scattering peak from Mie scattering is observed at 440 nm. (A scattering peak from coherent light scattering is observed at 760 nm) After coating with titanium oxide particles, the scattering peak shifts to a longer wavelength because the particle size is larger and the refractive index is higher. As shown in Figure 4-4 (b), the baseline is not change compared with Figure 4-4 (a). The possible cause is multiple light scattering from titanium oxide particles.

4-3-3. Optical properties of pellets composed of PMMA/TiO_2 particles

Aggregates composed of core-shell particles pressed by uniaxial pressurization are shown in Figure 4-5. Figure 4-5 (a) and Figure 4-5(b) show the results using PMMA

(a)

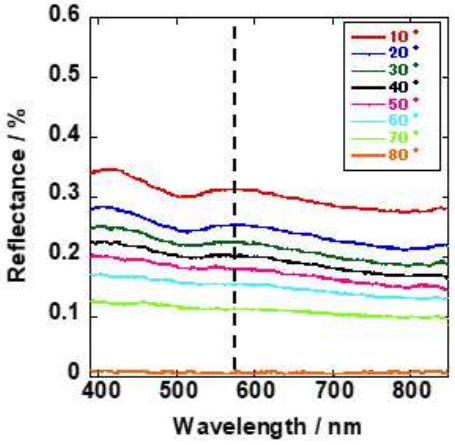

(b)

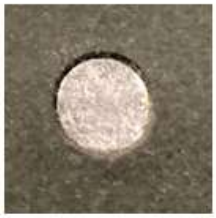

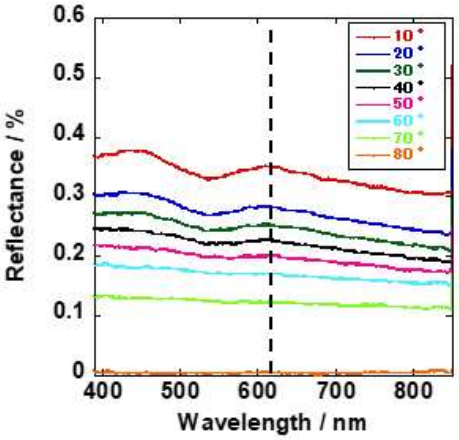

Figure 4-3. (a) A photograph and spectra of PMMA particle with particle size of average 400 nm. (b) A photograph and spectra of PMMA/ TiO_2 particles with Carbon black particles. (Particle size of PMMA particle = average 400 nm)

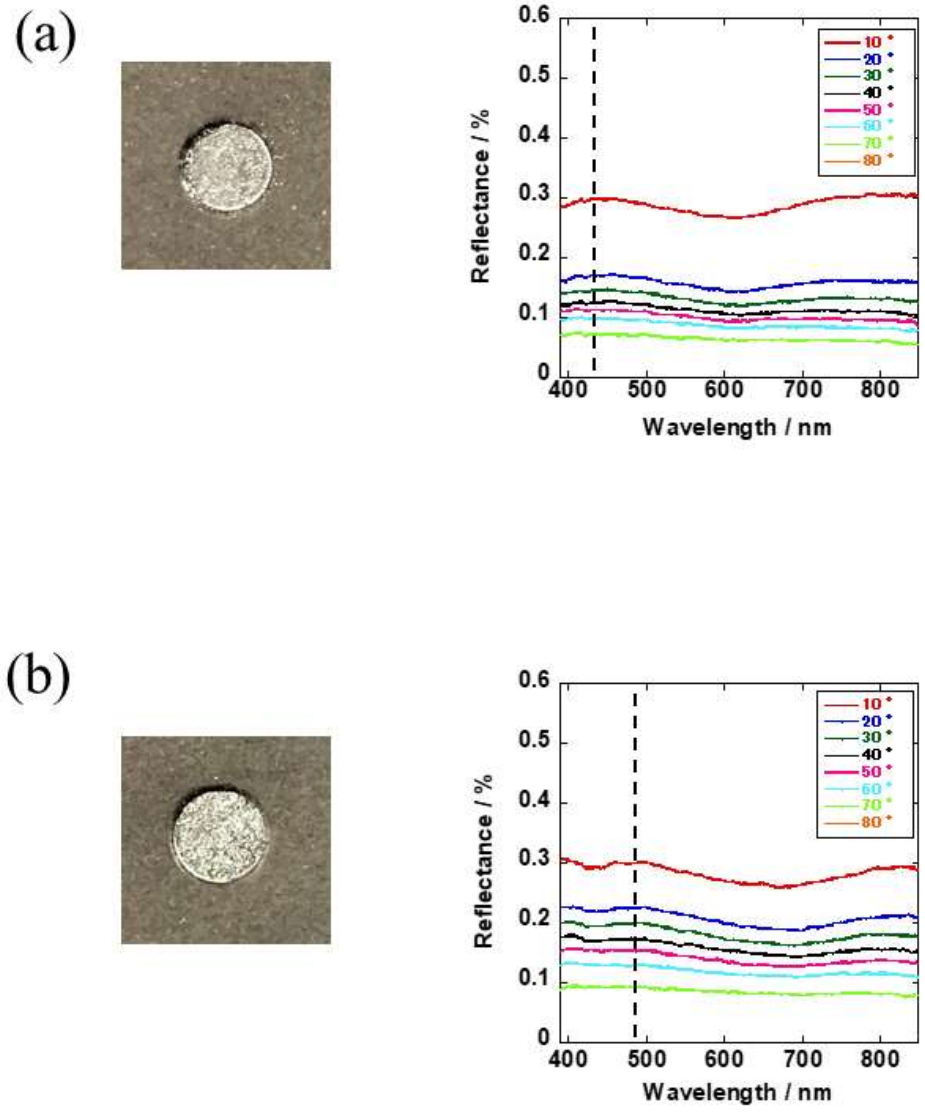

Figure 4-4. (a) A photograph and spectra of PMMA particle with particle size of average 350 nm. (b) A photograph and spectra of PMMA/ TiO_2 particles with Carbon black particles. (Particle size of PMMA particles = average 350 nm)

particles with particle size of average 400 nm and 350nm, respectively. The force ranged from 10 kN to 50 kN.

In case of PMMA particles with particle size of average 400 nm, the hue of the aggregates composed of PMMA/TiO_2 particles changed from red to purple to blue due to the pressing. Aggregates pressed over 30 kN show the same blue color.

In case of PMMA particles with particle size of average 350 nm, the hue of the aggregates composed of PMMA/TiO_2 particles changed from green to purple due to the pressing. Aggregates pressed over 30 kN show the same purple color.

According to this result, the cause of the same blue and purple color for the aggregates pressed over 30 kN is thought to be a lack of change in the particle form over 30 kN.

Then, a scattering spectrum from core-shell particles was compared with the spectra from pressed aggregates composed of core-shell particles (Figure 4-6). The scattering peak of the aggregate obtained by pressing with 10 kN is shifted from approximately 600 nm to 650 nm, and the reflectance spectrum on the shorter wavelength side is increased as shown in Figure 4-6 (a) and Figure 4-6 (b) (particle size of PMMA particles = average 400 nm). When an aggregate is pressed at 10 kN, Rayleigh scattering might just begin to occur and mix with Mie scattering in view of the aggregates showing a purple color and the spectrum. The scattering spectra of aggregates pressed over 20 kN show the same form, and the reflectance on the short wavelength side is increased.

In case of PMMA particles with size of average 350 nm, the spectra show results similar to Figure 4-6 (a) and Figure 4-6 (b) as shown in Figure 4-6(c) and Figure 4-6(d). The scattering peak of the aggregate obtained by pressing with 10 kN is shifted from

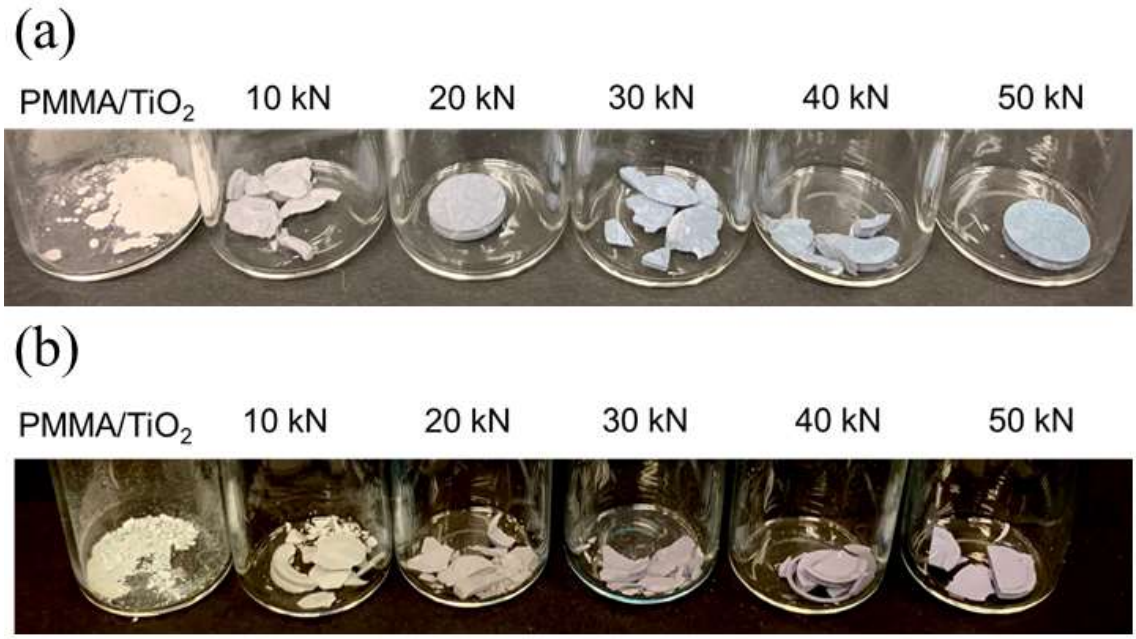

Figure 4-5. A photograph of PMMA/TiO_2 particles and aggregate composed of PMMA/TiO_2 particles pressed under 10 kN, 20 kN, 30 kN, 40kN, 50 kN. All samples contains carbon black particles due to decrease multiple scattering light.
(a) PMMA/TiO_2 particles using PMMA particles with particle size of average 400 nm. (b) PMMA/TiO_2 particles using PMMA particles with particle size of average 350 nm.

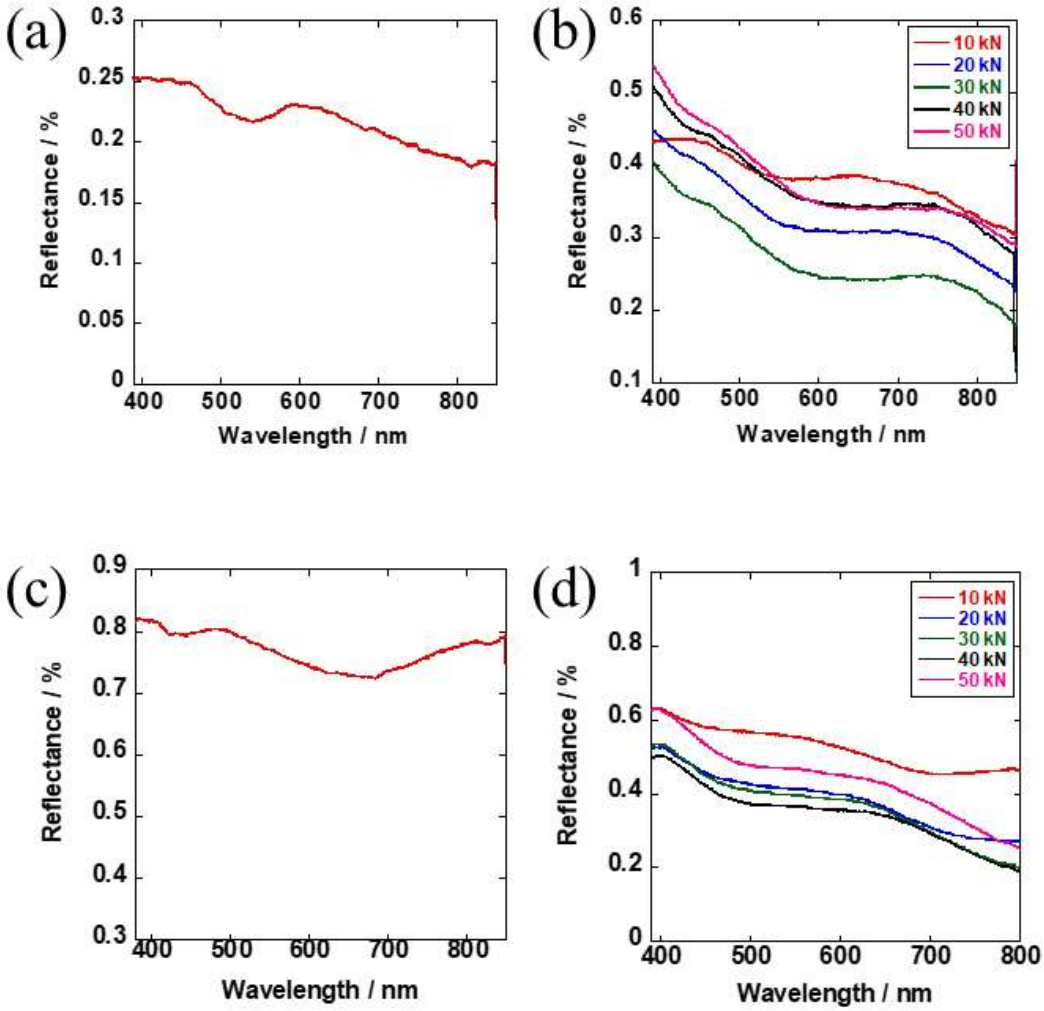

Figure 4-6. (a) A spectrum of PMMA/TiO_2 particles when viewing angle become 10° (Particle size of PMMA particles = average 400 nm). (b) Spectrum of the aggregates composed of PMMA/TiO_2 particles pressed under 10 kN, 20 kN, 30 kN, 40kN, 50 kN. (c) A spectrum of PMMA/TiO_2 particles when viewing angle become 10° (Particle size of PMMA particles = average 350 nm). (d) Spectrum of the aggregates composed of PMMA/TiO_2 particles pressed under 10 kN, 20 kN, 30 kN, 40kN, 50 kN.

approximately 490 nm to 550 nm, and the reflectance spectrum on the shorter wavelength side is increased. According to these results, a Rayleigh scattering effect occurs because the reflectance on the short wavelength side is uniformly increased.

The occurrence of Rayleigh scattering is due to scatterers smaller than the light wavelength. Rayleigh scattering is caused by the titanium oxide particles because their size is 7 nm; however, the scattered light does not show a blue color when only titanium oxide particles are present, instead showing a white color.

According to this fact, air gaps derived by pressing PMMA particles cause Rayleigh scattering, as I predicted.

Here, the spectrum of the aggregate composed of PMMA/TiO_2 particles obtained by pressing at 50 kN is compared with the spectrum of the aggregate composed of PMMA particles obtained by pressing at 50 kN (Figure 4-7). The blue line shows the spectra of the pressed aggregate of PMMA particles, and the red line shows the spectra of the pressed aggregate of PMMA/TiO_2 particles. Each aggregate contains 1 wt% CB particles to reduce multiple scattering of light. The reflectance on the short wavelength side for the aggregate of PMMA/TiO_2 particles is higher than that for the aggregate of PMMA particles. However, the reflectance on the short wavelength side for the aggregate of PMMA demonstrates an upward trend.

According to the general spectrum of Rayleigh scattering, Rayleigh scattering is definitely caused by the aggregate of only PMMA particles. The existence of air gaps (approximately 150 nm size) causing Rayleigh scattering was confirmed by observing an electron micrograph of the surface of a pellet composed of only PMMA particles (Figure

4-8(a)). Pellets composed of PMMA particles with a few CB particles and pressed from 10 kN to 50 kN show an ash color (Figure 4-8(b)). According to the results of Figure 4-6 and Figure 4-7, the blueshift with increasing pressure was caused by Rayleigh scattering, and this scattering occurred from not only the titanium oxide particles but also the air gaps due to the changing form of the PMMA particles.

However, according to Figure 4-8(b), the Rayleigh scattering caused by the air gaps did not contribute to the color of the aggregate. The Rayleigh scattering caused by the titanium particles is considered to largely contribute to the color.

4-3-4. Observation of the arrangement of PMMA/TiO_2 particles in the cross-section and on the surface of pellets

The existence of air gaps in pressed aggregates of PMMA/TiO_2 particles was confirmed by SEM observations. An electron micrograph and a Fourier transform image of a cross-section of an aggregate of PMMA/TiO_2 particles pressed at 50 kN are shown in Figure 4-9. The particles are deformed along the pressed direction. The deformed particles are not perfectly sealed. Air gaps appear in the aggregate, as I expected. The change in the surface of the aggregates of PMMA/TiO_2 particles pressed from 10 kN to 50 kN is shown in Figure 4-10. The PMMA/TiO_2 particles pressed at 30 kN or less exhibit a spherical form. However, the air gaps between particles began to be sealed at 40 kN and 50 kN. These electron micrographs clearly show that the air gaps were sealed and disappeared with the changing form of the particles under pressurization.

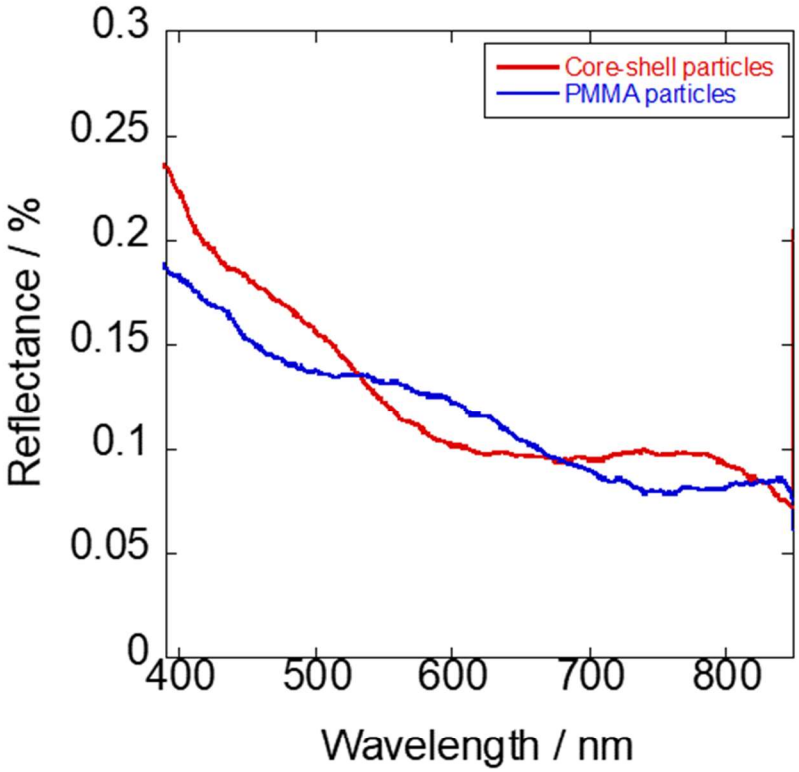

Figure 4-7. Comparison a pellet composed of PMMA particles and a pellet composed of PMMA/TiO_2 particles. (Particle size of PMMA particles = average 400 nm)

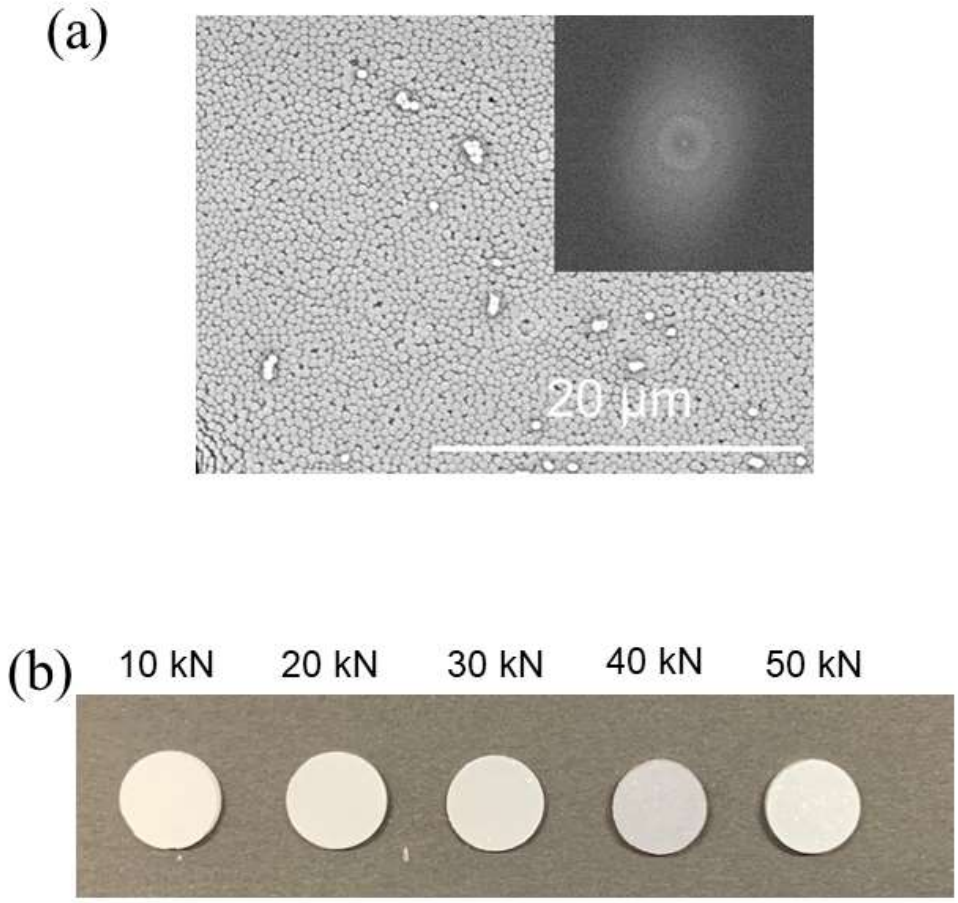

Figure 4-8. (a) Electron micro graph and its Fourier transform image of a surface of a pellet composed of PMMA particles. (b) A photograph of aggregates composed of PMMA particles pressed under 10 kN, 20 kN, 30 kN, 40kN, 50 kN. All samples contains carbon black particles. (Particle size of PMMA particles = average 400 nm)

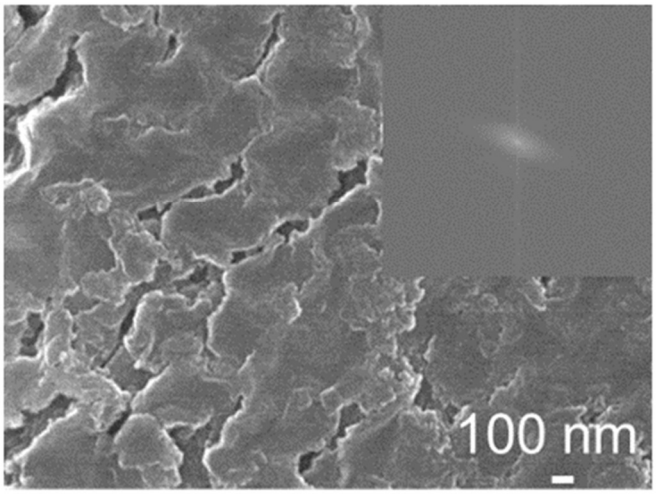

Figure 4-9. Electron micrograph and its Fourier transform image of cross-section of a pellet composed of PMMA/TiO_2 particles pressed under 50 kN. (Particle size of PMMA particles = average 400 nm)

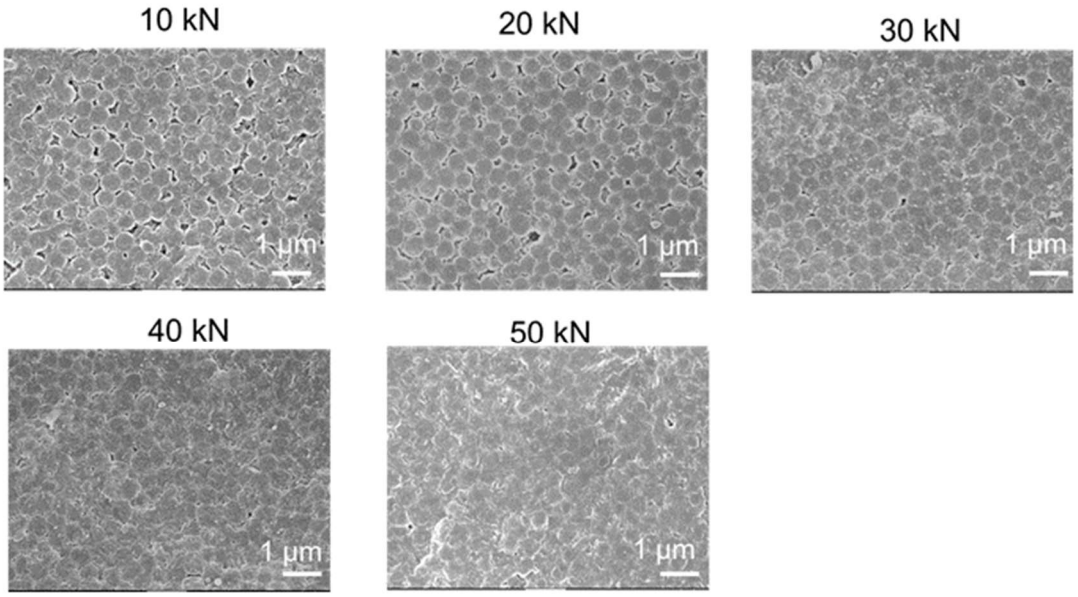

Figure 4-10. Electron micrograph of a pellet composed of PMMA/TiO_2 particles pressed under 10 kN, 20 kN, 30 kN, 40kN, 50 kN. (Particle size of PMMA particles = average 400 nm)

According to these results, the Rayleigh scattering caused by the titanium oxide particles largely contributes to the blueshift of the aggregates of PMMA/TiO_2 particles. Some possible mechanisms may cause the increase in the Rayleigh scattering and change in color with pressing of the PMMA/TiO_2 particles.

One of the possible causes is an increase in the number of titanium particles on the surface of the pellet due to pressing of the aggregate particles.

Another possible cause of the visualization of the Rayleigh scattering color is that titanium particles are uniformly dispersed in the aggregate. Uniform dispersion of titanium particles was found on the surface of a pellet composed of PMMA/TiO_2 particles, as revealed by the elemental mapping of titanium shown in Figure 4-11, which was obtained based on an electron micrograph.

From these results, the Rayleigh scattering derived from the titanium oxide particles is considered to greatly contribute to the color development of the Rayleigh scattering, and the uniform dispersion state of the titanium oxide particles led to the visualization of the color.

4-4. Conclusions

PMMA/TiO_2 core-shell particles were prepared by coating high refractive index titanium oxide particles on non-crosslinked PMMA particles. After that, the prepared PMMA/TiO_2 particles were pressed by uniaxial pressurization.

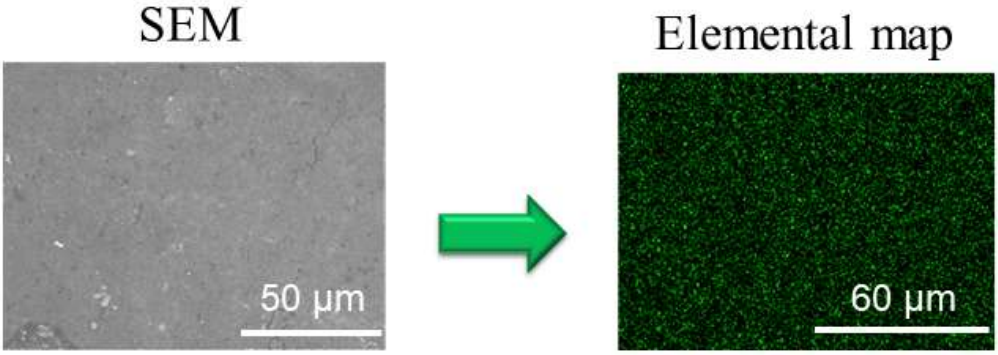

Figure 4-11. Electron micrograph of a pellet composed of PMMA/TiO_2 particles pressed under 10 kN, 20 kN, 30 kN, 40kN, 50 kN. (Particle size of PMMA particles = average 400 nm)

The hue of the aggregates of PMMA/TiO_2 particles blueshifted and the reflectance on the short wavelength side increased with increasing pressure. Colored materials based on Rayleigh scattering were prepared.

As a result, I report angle-independent colored materials with changing hue in response to pressure because of a phenomenon change from Mie scattering to Rayleigh scattering.

These prepared colored materials have conductive properties due to the presence of titanium oxide. Therefore, these materials may have new applications.

References

[1] L. Rayleigh, Scientific Papers, **5**, 617(1912).

[2] G. Mie, Ann. Phys., **25**, 377-455(1908).

[3] D. Ge, L. Yang, G. Wua and S. Yang, *J. Mater. Chem. C*,**2**, 4395-4400(2014).

[4] S-H. Kim, V. Hwang, S. G. Lee, J-W. Ha, V. N. Manoharan, and G-R. Yi, *Small*, **15**, 1900931 (2019).

[5] S. Cho, T. S. Shim, J. H. Kim, D-H. Kim, and S-H. Kim, *Adv. Mater.*, **29**, 1700256 (2017).

[6] W. Yuan, N. Zhou, L. Shi, and K-Q. Zhang, *ACS Appl. Mater. Interfaces*, **7**, 14064−14071 (2015).

[7] M. Retsch, M. Schmelzeisen, H-J. Butt, and E. L. Thomas, *Nano Lett.*, **11**, 1389–1394 (2011).

[8] L. A. Fielding, O. O. Mykhaylyk, A. Schmid, D. Pontoni, S. P. Armes, and P. W. Fowler, *Chem. Mater.*, **26**, 1270−1277 (2014).

[9] Y. Naoi, T. Seki, S. Yoshioka, Y. Takeoka, *Mol. Cryst. Liq. Cryst*., **688**, 105-113 (2019).

[10] Y. Naoi, T. Seki, R. Ohnuki, S. Yoshioka and Y. Takeoka, *Langmuir*, **35**, 13983-13990 (2019).

[11] D. Nakayama, Y. Takeoka, M. Watanabe, K. Kataoka, *Angew. Chem. Int. Ed.*, **42**, 4197-4200 (2003).

[12] Z. Cai, D. H. Kwak, D. Punihaole, Z. Hong, S. S. Velankar, X. Liu, S. A. Asher, *Angew. Chem. Int. Ed.*, **54**, 13036-13040 (2015).

[13] Md. A. Haque, G. Kamita, T. Kurokawa, K. Tsujii. J. P. Gong, *Adv. Mater.*, **22**, 5110-5114 (2010).

[14] S. Furumi, H. Fudouzi, and T. Sawada, *Laser & Photon*., **4**, 205–220 (2010).

[15] W. Lu, H. Li, B. Huo, Z. Meng, M. Xue, L. Qiu, S. Ma, Z. Yan, C. Piao, X. Ma, *Sensors and Actuators B*, **234**, 527-533.

[16] Y. Ohtsuka, T. Seki, Y. Takeoka, *Angew. Chem. Int. Ed.*, **54**, 15368-15373 (2015).

[17] S. Nagaoka, M. Nagata, K. Arinaga, K. Shigemori, M. Takafujic and H. Iharac, *Color. Technol.*, **123**, 344–350 (2007).

[18] R. A. Caruso, A. Susha, and F. Caruso, *Chem. Mater.*, **13**, 400-409 (2001).

[19] H. Xu, X. Chen, S. Ouyang, T. Kako, and J. Ye, *J. Phys. Chem. C*, **116**, 3833−3839 (2012).

[20] H. Nakamura, M. Ishii, A. Tsukigase, M. Harada, H. Nakano, *Langmuir*, **21**, 8918-8922 (2005).

[21] T. Shirosaki, E. Tsuda, M. Horikawa, S. Nagaoka, and H. Ihara, *Color. Technol.*, **133**, 187–193 (2017).

[22] K. Furusawa, K. Nagashima, C. Anzai, *Kobunshi Ronbunshu*, **50**, 343-347 (1993).

Chapter V

Angle-Independent Colored Materials with Colloidal Crystals Composed of CeO_2/PVP Particles

5-1. Introduction

Colloidal amorphous arrays have been reported to work as angle-independent colored materials under natural light, a fact that is known today[1-21]. However, the scattering spectrum of a colloidal amorphous array is broad. Therefore, the color is pale.

In contrast, colloidal crystals[22-26] have long-range order and reflect specific light with a wavelength comparable to the size order. Therefore, the color is brighter than the color of colloidal amorphous arrays. However, the color changes with viewing angle and irradiation angle because the structures have anisotropy.

If angle-independent colored materials could be prepared from colloidal crystals, then brilliant colored materials that are extraordinarily easy to use could be prepared.

The Bragg-Snell law is used to determine the wavelength of light scattered from colloidal crystals as follows.

$$\lambda = 2d(n^2 - \cos\theta^2)^{1/2}$$

where d denotes the lattice spacing, n denotes the average refractive index of the colloidal crystal and θ denotes the incident angle. According to this law, the effect of the viewing angle can be decreased by increasing the refractive index of the particles composing the colloidal crystal. In other words, colloidal crystals showing a color with low angle dependence could be prepared by using high refractive index particles.

In this research, we prepared colloidal crystals showing angle-independent color by using high refractive index CeO_2/PVP particles. CeO_2 has a high refractive index (refractive index = 2.2). However, the dispersibility is not good. The CeO_2/PVP particles used in this research overcome this defect by coating with PVP, which has excellent dispersibility. Moreover, PVP is a food-grade-safe material. Angle-independent colored materials obtained by using CeO_2/PVP particles could be used as safe pigments in our lives.

In this chapter, the aims of this research are to prepare colloidal crystals showing angle-independent color.

Thus, colloidal crystals showing angle-independent color are successfully prepared by evaporating a water suspension of CeO_2/PVP.

5-2. Experimental section

5-2-1. Materials

Water suspensions of CeO_2/PVP core-shell particles were provided by Hokko Chemical Co., Ltd. The average particle size was 200 nm (10.1 wt%).

Monodisperse fine silica particles (2.3 g/cm^3) with an average diameter of 197 were purchased from Fuji Chemical Co., Ltd. for use in this study.

5-2-2. Preparation of colloidal crystals of CeO_2/PVP particles

A water suspension of CeO_2/PVP core-shell particles (400 μl) was poured into a plastic case. The suspension was left at room temperature for a prolonged period, and colloidal crystals composed of CeO_2/PVP core-shell particles were prepared.

5-2-3. Scattering spectrum measurements

The angle dependence of the scattering spectrum and specular reflection spectrum were determined by means of a UV-vis spectrometer (Nippon Bunko Company, V-670) and a goniometer (ARMN-735)

When the angle dependence was measured, the light was incident from a direction perpendicular to the flat surface of the sample, the detector was placed at various angular positions relative to the incident direction, and the scattering spectrum was measured.

The specular reflection spectra were measured by changing the angle between the incident light and detector from 10° to 100° (the incident angle and viewing angle were the same).

5-2-4. Observation of electron microscope images

Colloidal crystals and films of CeO_2/PVP core-shell particles were observed using a scanning electron microscope (JEOL, JSM-7500FA). Samples were coated with a 5 nm osmium layer using a magnetron sputtering apparatus, and the images were acquired using SEM operated at 15 kV (Filgen, OPC60A).

5-2-5. Optical pictures obtained with a digital camera

Photographs of prepared composite particles and pellets were taken with an iPhone 6s.

5-3. Results and discussion

Angle dependence of colloidal crystals of CeO_2/PVP particles

A prepared colloidal crystal of CeO_2/PVP particles is shown in Figure 4-1(a). The colloidal crystal displays a shiny red color. Diffuse scattering spectra were measured to evaluate the angle dependence of the color derived from the colloidal crystal. The results are shown in Figure 4-1(b). The scattering peak at 620 nm is the scattering peak causing the red color. The peak shifts to a short wavelength with increasing viewing angle; however, the mobility of the peak is small. When the viewing angle is 10°, the scattering peak is positioned at 620 nm, and when the viewing angle is 20°, the peak shifts to 619 nm; when the viewing angle is 30°, the peak shifts to 617 nm.

Then, a colloidal crystal composed of fine silica particles with a size of 197 nm was prepared for comparison with the colloidal crystal composed of CeO_2/PVP particles.

In the case of the scattering peak derived from the silica colloidal crystal, the peak (coherent light scattering) dramatically shifts to a shorter wavelength with increasing viewing angle, as shown in Figure 4-2.

In contrast, the scattering peak of the CeO_2/PVP colloidal crystal shifts to a shorter wavelength by only a few nanometers. As I expected, a colored material with low angle dependence was obtained.

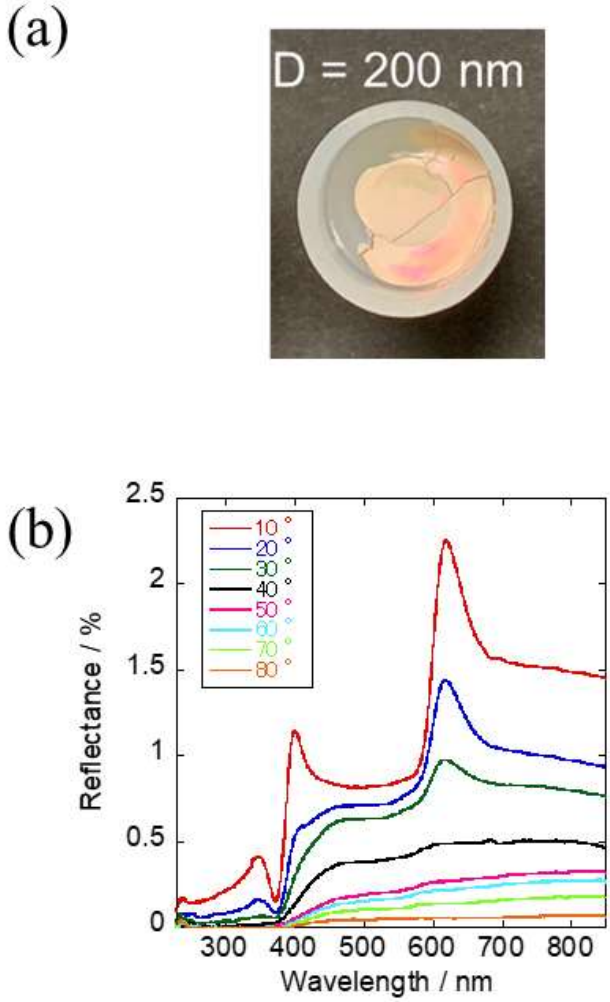

Figure 4-1. (a) A photograph of colloidal crystal of CeO_2/PVP particles (d = 200 nm). (b) Angular dependence of spectrum of colloidal crystal of CeO_2/PVP particles (d = 200 nm).

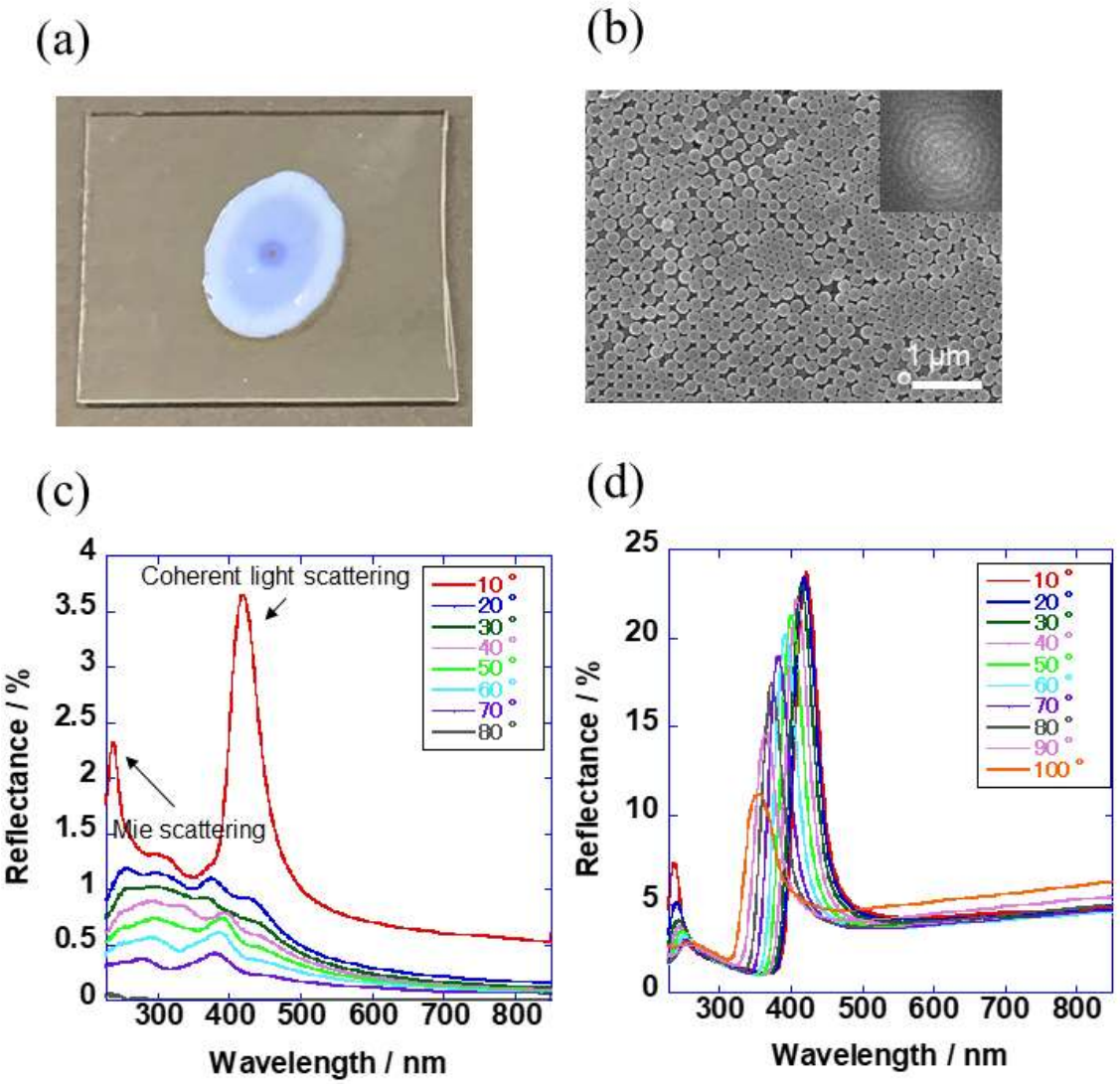

Figure 4-2. (a) A photograph of colloidal crystal composed of silica particles (d = 200 nm). (b) Electron micrographs of prepared colloidal crystal. (c) Angular dependence of spectrum of colloidal crystal. (d) Spectrum of secular reflection of prepared colloidal crystal.

In Figure 4-1(b), two angle-independent scattering peaks are observed at 340 nm and 402 nm. These scattering peaks do not contribute to the color of the colloidal crystal because the intensity is lower than that of the scattering peak on the long wavelength side.

Then, specular reflection spectra were measured to confirm that the origin of the peaks obtained from the colloidal crystal is the structure. The angle between the incident light and detector was changed from 10° to 100° (the incident angle and viewing angle were the same), and the measured specular reflection spectra are shown in Figure 4-3. If the scattering spectra were derived from the structure of the colloidal crystal, then the scattering peaks would shift to a shorter wavelength with increasing viewing angle depending on the Bragg-Snell law (as shown in Figure 4-2 (d)). In Figure 4-3, the scattering peak positioned at 620 nm shifts to a shorter wavelength with increasing angle. Therefore, this scattering peak is derived from the structure of the colloidal crystal.

In contrast, the two scattering peaks on the short wavelength side show a different behavior than the scattering peak derived from the colloidal crystal. The two scattering peaks redshift with increasing angle between the incident light and detector. In case of a colloidal crystal composed of silica particles as shown in Figure 4-2 (d), the scattering peak from Mie scattering shows similar spectra. According to Figure 4-2 (d) and Figure 4-3, the two scattering peaks were from the Mie scattering occurring from the colloidal crystal.

Then, the arrangement of the CeO_2/PVP particles of the colloidal crystal was observed by electron microscopy (Figure 4-4). The Fourier transform image is shown in the inset

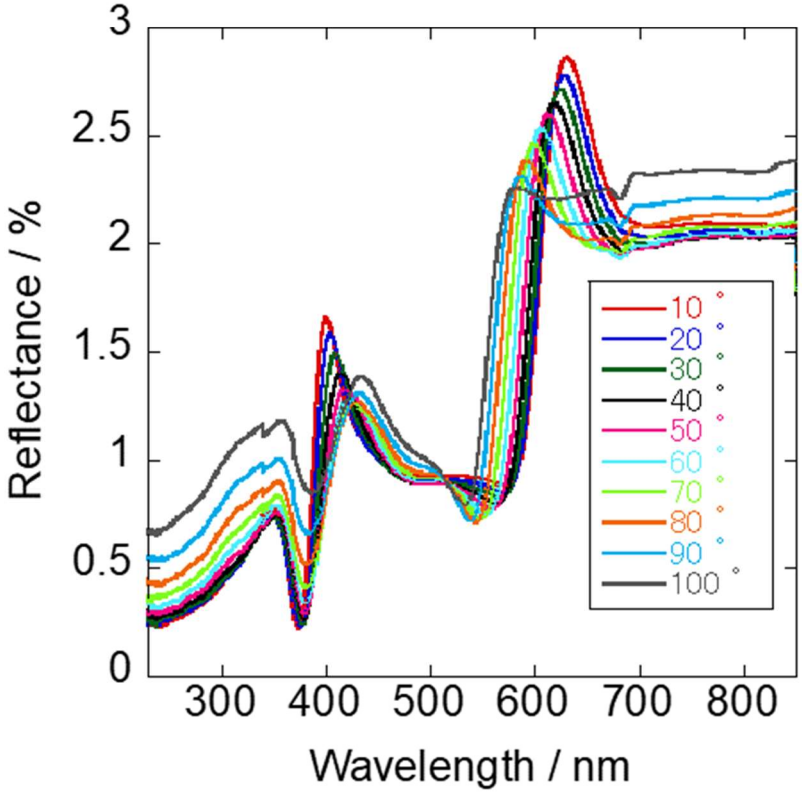

Figure 4-3. Spectrum of secular reflection of prepared colloidal crystal of CeO_2/PVP particles (d = 200 nm).

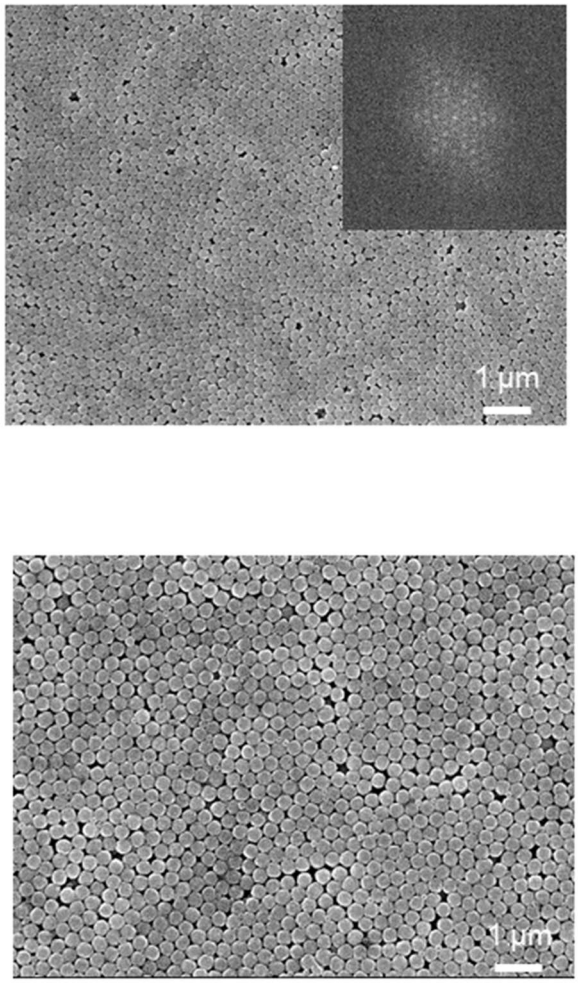

Figure 4-4. Electron micrographs of prepared colloidal crystal of CeO_2/PVP particles (d = 200 nm).

image. The CeO_2/PVP particles are arranged with long-range order and form a colloidal crystal.

As these results show, a colloidal crystal with low angle dependence was obtained by using high refractive index CeO_2/PVP particles.

5-4. Conclusion

An angle-independent colored material was prepared by forming a colloidal crystal composed of high refractive index CeO_2/PVP particles.

A shiny angle-independent colored material was obtained because the reflectance is high when using the colloidal crystal.

References

[1] Y. Takeoka, M. Honda, T. Seki, M. Ishii, H. Nakamura, *ACS Appl. Mater. Interfaces*, 2009, **1**, 982-986.

[2] M. Harun-Ur-Rashid, A. Bin. Imran, T. Seki, M. Ishi, H. Nakamura, Y. Takeoka, *ChemPhysChem*, 2010, **11**, 579-583.

[3] J. D. Forster, H. Noh, S. F. Liew, V. Saranathan, C. F. Schreck, L. Yang, J. G. Park, R. O. Prum, S. G. J. Mochrie, C. S. O'Hern, H. Cao, E. R. Dufresne, *Adv. Mater.*,2010, **22**, 2939-2944.

[4]. Garcia, P. D.; Sapienza, R.; Lopez, C., *Adv. Mater.*, 2010, **22** (1), 12-19.

[5] I. Lee; D. Kim; J. Kal.; H. Baek; D. Kwak; D. Go; E. Kim; C. Kang; J. Chung; Y. Jang; S. Ji; J. Joo; Y. Kang, *Adv Mater.*,2010, **22** (44), 4973-4977.

[6] S. F. Liew, J. Foster, H. Noh, C. F. Schreck, V. Saranathan, X. Lu, L. Yang, R. O. Prum, C. S. O'Hern, E. R. Dufresne, H Cao, *Opt. Express*, 2011, **19**, 8208-8217.

[7] Y. Takeoka, S. Yoshioka, A. Takano, S. Arai, N. Khamin, H. Nishihara, M. Teshima, Y. Ohtsuka, T. Seki, *Angew. Chem. Int. Ed.*, 2013, **52**, 7261-7265.

[8] L. Shi.; Y. F. Zhang; B. Q. Dong; T. R. Zhan; X. H. Liu; J. Zi, *Adv. Mater.*, 2013, **25** (37), 5314-5320.

[9] S. Yoshioka and Y. Takeoka, *ChemPhysChem*, 2014, **15**, 2209-2215.

[10] S. Magkiriadou, J-G. Park, Y-S. Kim, and V. N. Manoharan, *Phys. Rev. E.*, 2014, **90** (6).

[11] D. Ge, L. Yang, G. Wua and S. Yang, *J. Mater. Chem. C*, 2014, **2**, 4395-4400.

[12] D. Montesdeoca; F. Bayat; A. Espinha; A. Blanco; C. Pecharroman; C. Lopez, *Part Part Syst Char*., 2016, **33** (12), 871-877.

[13] I. Yoo; J. Hyon; S. Song; Y. Kang, *Sci. Adv. Mater.*, 2017, **9** (2), 238-243.

[14] G. J. Aubry; L. Schertel; M. D. Chen; H. Weyer; C. M. Aegerter; S. Polarz; H. Colfen; G. Maret, *Phys. Rev. A.*,2017, **96** (4).

[15] M. Iwata.; M. Teshima.; T. Seki; S. Yoshioka; Y. Takeoka, *Adv. Mater.*, 2017, **29** (26).

[16] K. Katagiri; Y. Tanaka; K. Uemura.; K. Inumaru; T. Seki; Y. Takeoka, *Npg. Asia. Mater.*, 2017, **9**. 28.

[17] P. Shi; F. Wang; J. F. Zhu; H. B. Yang; Y. Wang; Y. Fang; B. Zhang.; J. H. Wang, *J. Eur. Ceram. Soc.*, 2018, **38** (4), 2228-2233.

[18] S. Y. Lee; H. Kim; S. H. Kim; , H. A. Stone, *Phys. Rev. Appl.*, 2018, **10** (5).

[19] G. L. Shang; L. Maiwald, H. Renner; D. Jalas; M. Dosta; S. Heinrich; A. Petrov; M.

Eich, *Sci Rep.*, 2018, **8**, 7894.

[20] L. Schertel; L. Siedentop; J. M. Meijer; P. Keim; C. M. Aegerter; G.J. Aubry.;G. Maret, *Adv. Opt. Mater.*, 2019, **7** (15).

[21] M. Kohri; Y. Tamai; A. Kawamura; K. Jido; M. Yamamoto; T. Taniguchi; K. Kishikawa; S. Fujii; N. Teramoto; H. Ishii; D. Nagao, *Langmuir*, 2019, **35** (16), 5574-5580.

[22] M. Kohri, *Polym J.,* 2019, **51**, 1127–1135.

[23] Y. N. Xia , B. Gates , Y. D. Yin and Y. Lu , *Adv. Mater*., 2000, **12** , 693 -713.

[24] Y. N. Xia , B. Gates and Z. Y. Li , *Adv. Mater*., 2001, **13** , 409 -413.

[25]] Y. Z. A. Zhang , J. X. Wang , Y. Huang , Y. L. Song and L. Jiang , *J. Mater. Chem*., 2011, **21,** 14113 -14126.

[26] S. H. Kim , S. Y. Lee , S. M. Yang and G. R. Yi , *NPG Asia Mater.*, 2011, **3** , 25 -33.

Appendix

Optical properties of prepared films composed of CeO_2/PVP particles

In the case of the preparation of an aggregate composed of CeO_2/PVP particles, stronger visualization of light scattered by Mie scattering (or Mie resonances) than in the case of silica particles is expected to be observed.

In chapter III, the effect of Mie scattering by aggregates was revealed. Thus, I expected that the light scattered by Mie scattering could be more clearly observed by using high refractive index CeO_2/PVP particles than by using silica particle. I performed this experiment and show the results in the appendix.

Materials

Water suspensions of CeO_2/PVP core-shell particles were provided by Hokko Chemical Co., Ltd. The average particle size was 200 nm (10.1 wt%) and 250 nm (10.1 wt%).

Preparation of films of CeO_2/PVP particles

Films of CeO_2/PVP particles were prepared by spin coating[1-3]. Spin coating has been established as a method that can prepare uniform films and control the thickness over a large area. In this research, the films were prepared in three steps by changing the spinning rate and rotation time: 1: suspension spreading, 2: suspension thinning, and 3: evaporation of water. First, a water suspension of CeO_2/PVP particles (50 μl) was deposited on a glass slide. In the case of preparing a film with a broad interparticle distance, the spinning rate of the first step was 1900 rpm, the spinning rate of the second step was 2500 rpm, and the

spinning rate of the third step was 5200 rpm. The rotation time was 3 seconds for each step. In the case of preparing a film with a narrow interparticle distance, the spinning rate of the first step was 1600 rpm, the spinning rate of the second step was 2700 rpm, and the spinning rate of third three step was 4200 rpm. The rotation time was 8 seconds for each step.

Results

In chapter III, the fact that Mie scattering was influenced by aggregates was revealed.

In this research, the result that Mie scattering is significantly affected by the structure of the aggregate is expected because the intensity would be higher when using particles with a higher refractive index than silica.

Here, a film with a broad interparticle distance and a film with a narrow interparticle distance composed of CeO_2/PVP particles were formed, and the optical properties were evaluated. Based on the reported method, the film with a broad interparticle distance was prepared by spin coating a glass slide with a water suspension of CeO_2/PVP particles at high speed for a short time. Then, the film with a narrow interparticle distance was prepared by spin coating a glass slide with a water suspension of CeO_2/PVP particles at low speed for a long time.

The scattering spectra, optical photographs and electron micrographs of each film are shown in Figure A1 and Figure A2. When the particle size is 200 nm, the intensity of the scattering peak at 402 nm derived from the film with a narrow interparticle distance (Figure A1(d)) is higher than that of the same peak derived from the film with a broad

interparticle distance (Figure A1(a)). Moreover, the intensity of the peak at 300 nm from the Mie scattering of the film with a broad interparticle distance is significantly higher than that of the same peak of the film with a narrow interparticle distance. In other words, clear differences could be observed in the intensities of the Mie scattering between the film with a broad interparticle distance and the film with a narrow interparticle distance. An optical photograph of the film with a broad interparticle distance is shown in Figure A1(b). An optical photograph of the film with a narrow interparticle distance is shown in Figure A1(d). The optical photograph of the film with a broad interparticle distance displays a purple color. In contrast, the optical photograph of the film with a narrow interparticle distance displays a blue-purple color. The reason is that the intensity of the scattering peak at 403 nm from Mie scattering for the film with a broad interparticle distance is lower than that of the peak for the film with a narrow interparticle distance, and the peak at 620 nm causing the red color derived from the structure affects the overall color.

Electron micrographs of each film with a broad interparticle distance and a narrow interparticle distance are shown in Figure A1(c) and Figure A1(f). The CeO_2/PVP particles of the film with a broad interparticle distance and the film with a narrow interparticle distance are arranged like a colloidal amorphous array with long-range order. The interparticle distance of the CeO_2/PVP particles composing the film with a broad interparticle distance is greater than the distance of the film with a narrow interparticle distance. The reason is thought to be that CeO_2/PVP particles were ejected when the film with a broad interparticle distance was prepared because the rotation speed was high and

the attachment of the CeO_2/PVP particles was weak. The possibility that the intensity of the Mie scattering peaks was affected by the interparticle distance was suggested by this result.

For a particle size of 250 nm, a film with a broad interparticle distance and a film with a narrow interparticle distance were prepared using the same method. The scattering spectra, optical photographs and electron micrographs of each film are shown in Figure A2. The scattering peak derived from the structure in the infrared light range does not contribute to the color of the film. Three Mie scattering peaks derived from the aggregates are found at 466 nm, 395 nm and 308 nm on the short wavelength side. The scattering peaks of the film with a broad interparticle distance (Figure A2(a)) were compared with the peaks of the film with a narrow interparticle distance (Figure A2(b)). In the film with a broad interparticle distance, the intensities of the two scattering peaks on the shorter wavelength side are higher; however, in the film with a narrow interparticle distance, the intensity of the peak on the longer wavelength side is higher.

In the compared optical photographs, each color is blue because the intensity of the scattering peak at 395 nm is high. Based on a comparison of the electron micrographs, the interparticle distance of the film with a broad interparticle distance is greater than the distance of the film with a narrow interparticle distance, as in the case of a particle size of 200 nm. Thus, the interparticle distance of aggregates is thought to affect the intensity of the Mie scattering.

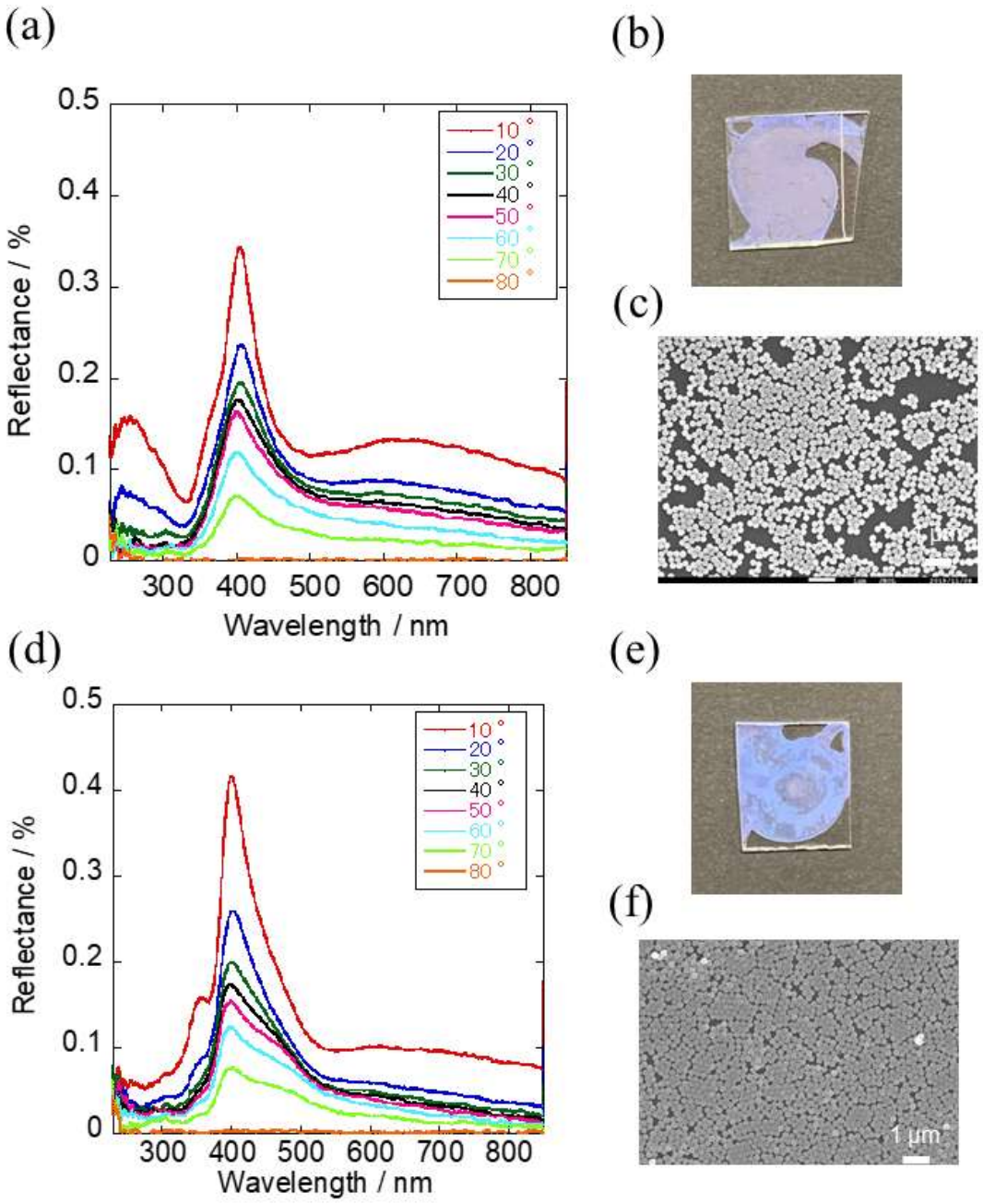

Figure A1 (a) Angular dependence of spectrum of film having broad interparticle distance of CeO_2/PVP particles (d = 200 nm). (b) A photograph of (a). (c) A electron micrograph of (a). (d) Angular dependence of spectrum of film having narrow interparticle distance of CeO_2/PVP particles. (e) A photograph of (d). (f) A electron micrograph of (d).

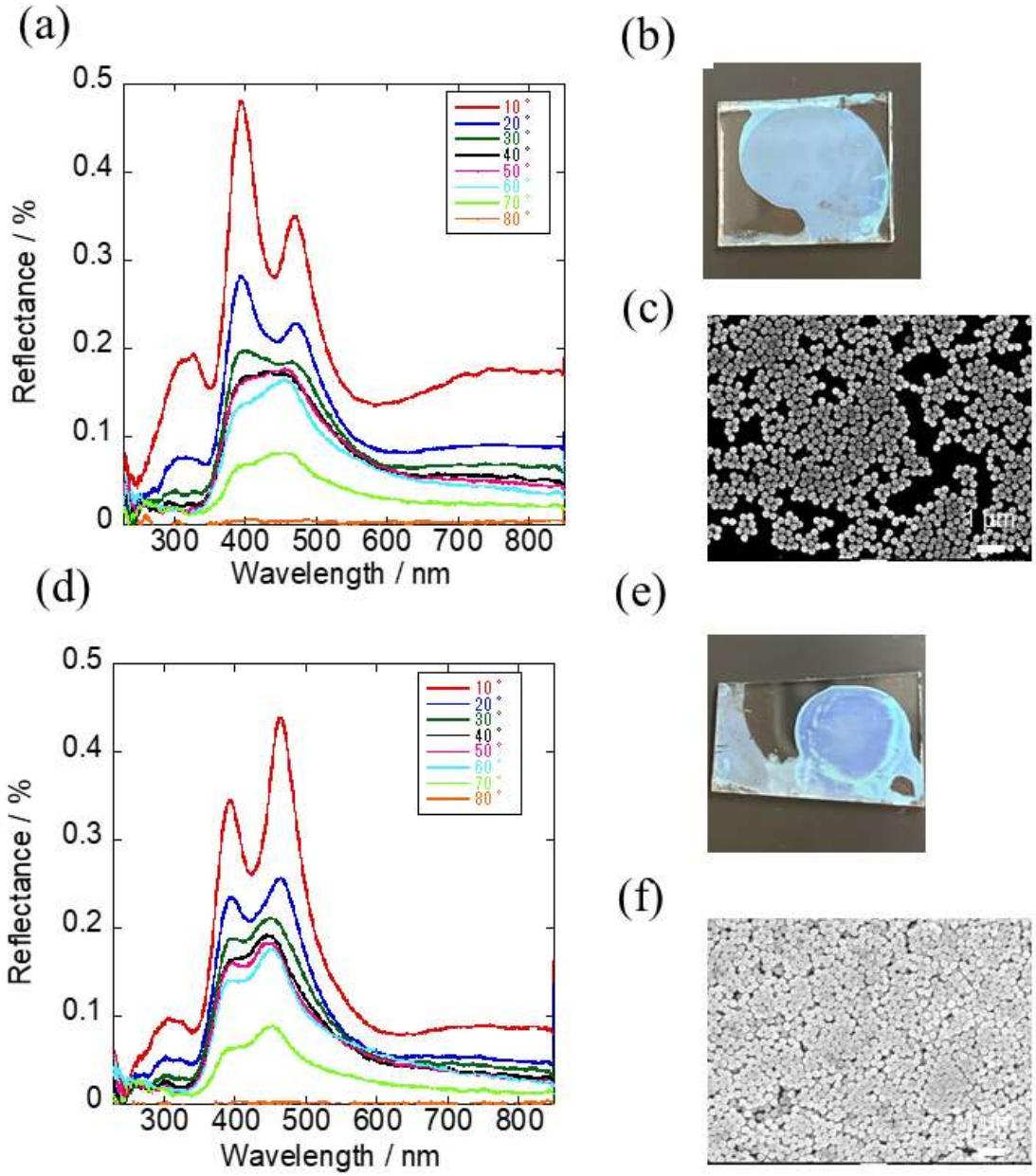

Figure A2 (a) Angular dependence of spectrum of film having broad interparticle distance of CeO_2/PVP particles (d = 250 nm). (b) A photograph of (a). (c) A electron micrograph of (a). (d) Angular dependence of spectrum of film having narrow interparticle distance of CeO_2/PVP particles. (e) A photograph of multi-layer film of (d). (f) A electron micrograph of(d).

Chapter VI

Summary and Outlook

This thesis has presented a new design approach for preparing angle-independent colored materials by using various scattering phenomena.

In chapter II, the fact that the scattering peaks caused by Mie scattering affected by aggregates showed angle independence was discovered.

Moreover, angle-independent colored materials were successfully prepared by positioning the Mie scattering peak caused by colloidal aggregates in the visible light range based on the Mie scattering property.

In chapter III, I focused on the effect that occurs when particles causing Mie scattering form aggregates. Then, the scattering spectra for the Mie scattering caused by an independent single particle were compared with the scattering spectra for the Mie scattering caused by colloidal aggregates. An association between Mie scattering and colloidal aggregates was revealed because the intensity and position of the peak from Mie scattering caused by colloidal aggregates were different from those in the spectra of Mie scattering caused by an independent single particle. As a result, the angle dependence was concluded to disappear upon the formation of aggregates composed of particles causing Mie scattering.

In addition, I found that anisotropy was induced in the short-range order by uniaxially compressing fine particles, which reduced the angle dependence when viewed from the compression surface. Research reporting that the induction of anisotropy in short-range

order structures influences the angle dependence has never been reported. This thesis could provide new insights into the design of structural color materials.

In chapter IV, an angle-independent colored material with changing hue in response to pressure was prepared by compressing PMMA/TiO_2 particles.

The color could be changed by switching from Mie scattering to Rayleigh scattering.

In chapter V, a colloidal crystal composed of high refractive index CeO_2/PVP particles was obtained based on the Bragg-Snell law determining the wavelength of light scattered by a colloidal crystal. As intended, colloidal crystals displaying angle-independent color were prepared.

This research theme suggests the possibility of expanding the range of use of colored materials based on light scattering, interference, and resonance phenomena. This theme opens the door to methods for both suppressing the angle dependence and achieving a brilliant color. Moreover, the mechanism behind the suppression of the angle dependence of structural color materials was revealed.

These results will help in applying structural color materials to industry such as in pigments and sensors.

Publications

1. Yui Naoi, Takahiro Seki, Shinya Yoshioka, Yukikazu Takeoka, “Development of angle-independent color material using colloidal amorphous array”, *Mol. Cryst. Liq. Cryst.*, **688**, 105-113 (2019).

2. Yui Naoi, Takahiro Seki, Ryosuke Ohnuki, Shinya Yoshioka, Yukikazu Takeoka, “Characterization of Colloidal Amorphous Arrays Prepared by Uniaxial Pressure Application”, *Langmuir*, **35**, 13983-13990 (2019).

3. Yui Naoi, Takahiro Seki, Yukikazu Takeoka, “Angle-Independent Colored Materials with Mie Scattering and Rayleigh Scattering in Response to Pressure”, in preparation.

4. Yui Naoi, Miki Sakai, Takahiro Seki, Yukikazu Takeoka, “Angle-Independent Colored Materials with Colloidal Crystals Composed of CeO_2/PVP Particles”, in preparation.

Presentations at International Conferences

1. Yui Naoi, Yukikazu Takeoka, Takahiro Seki, “Preparation of angle-independent color materials by applying Mie resonances”, 255th ACS National Meeting, New Orleans, LA, U.S.A (2018).

2. Yui Naoi, Yukikazu Takeoka, Takahiro Seki, “Optical devices by Mie resonances”, The 22th International Symposium on Advanced Display Materials and Devices (ADMD 2018), Jeju-do, Korea (2018).

3. Yui Naoi, Yukikazu Takoka, Takahiro Seki, “Angle-independent color materials by Mie resonances”, 2018 KJF International Conference on Organic Materials for Electronics and Photonics (KJF-ICOMEP 2018), Nagoya, Japan (2018).

4. Yui Naoi, Yukikazu Takeoka, Takahiro Seki, “Angle-independent photonic pigments by Mie resonances from dielectric colloidal aggregates”, 2018 MRS Fall Meeting & Exhibit, Boston, U.S.A (2018).

5. Yui Naoi, Yukikazu Takeoka, Takahiro Seki, “New photonic materials by Mie resonances”, The 12th SPSJ International Polymer Conference (IPC 2018), Hiroshima, Japan (2018).

Acknowledgements

This thesis is based on the studies under Prof. Takahiro Seki at the Department of Molecular and Macromolecular Chemistry, Graduate School of Engineering, Nagoya University.

First of all, I would like to express my deepest appreciation to my supervisor Prof. Takahiro Seki for his helpful guidance and encouragement throughout my doctorates course, as well as for providing a lot of valuable opportunities to participate in conferences and research. I would like to show my gratitude to the laboratory staffs, Assoc. Prof. Yukikazu Takeoka, Assoc. Prof. Shusaku Nagano and Assist. Prof. Mitsuo Hara for their sincere discussions, as well as detailed guidance and advice on experiments and measurements. I am particularly grateful to Assoc. Prof. Yukikazu Takeoka that helped my research in the right direction and brushed up it.

This thesis was also supported by many researcher's helps in other research institutions. Many thanks to Assoc. Prof. Shinya Yoshioka (Tokyo University of Science) and Mr. Ryosuke Ohnuki for all the valuable discussions and productive collaborations.

I could not have performed my research works without their supports.

I wish to express my special thanks to all members of the Seki laboratory including alumni for their generous supports, encouragements and friendships. In particular, I would like to thank Mr. Kenta Watanabe, Ms. Yuumi Okaya, Mr. Dowoo Kwon, Mr. Eiji Miwa, Mr. Yusuke Baba, Mr. Ikuya Ohshima, Mr. Tomoki Sakai, Mr. Suzhe Liu, Ms. Yuwen Ai, Ms. Yuuka Hiei, Ms. Shi Pei, Dr. Jeremy Odent, Mr. Fumio Asai, Mrs. Yumiko Ohtsuka, Mrs. Miki Sakai. I received various cooperation and warm encouragement in my laboratory life from Mrs. Yuko Ohiwa as administrative assistant and Dr. Koji Mukai and Mr. Issei kitamura. I appreciate them sincerely.

Finally, I am grateful to my family, and my friends for their heartfelt encouragement, understanding, and helpful supports.

March, 2020
Yui Naoi